# Sliding wear behaviour of HVOF and HVAF sprayed $Cr_3C_2$-based coatings

V. Matikainen[1*], G. Bolelli[2], H. Koivuluoto[1], P. Sassatelli[2], L. Lusvarghi[2], P. Vuoristo[1]

[1] Tampere University of Technology, Korkeakoulunkatu 6, Tampere, Finland.
[2] University of Modena and Reggio Emilia, Via Pietro Vivarelli 10/1, Modena, Italy.

## Abstract

Thermally sprayed tungsten carbide (WC) and chromium carbide ($Cr_3C_2$) based hard metal coatings are commonly applied on component surfaces as corrosion and wear resistant layers. Typically, WC-Co/Ni with optional Cr addition and $Cr_3C_2$-25NiCr powders are sprayed with high velocity oxy-fuel (HVOF) or high velocity air-fuel (HVAF) processes. Due to the poor oxidation resistance of the WC particles, $Cr_3C_2$-25NiCr composition is typically selected for high temperature environments, up to 800-900 °C. In this study, two distinct $Cr_3C_2$-based compositions of $Cr_3C_2$-50NiCrMoNb and $Cr_3C_2$-37WC-18NiCoCr were selected as interesting alternatives to conventional $Cr_3C_2$-25NiCr. Sliding wear behavior of the coatings sprayed with HVOF and HVAF processes were tested with a ball-on-disk configuration against an $Al_2O_3$ ball at room temperature and at 700 °C. It was found that both alternative materials had comparable coefficients of friction with the $Cr_3C_2$-25NiCr coatings. The $Cr_3C_2$-37WC-18NiCoCr coatings provided improved wear resistance at room temperature conditions, but at 700 °C the wear rate was increased to the level of the $Cr_3C_2$-50NiCrMoNb coatings. $Cr_3C_2$-25NiCr coatings experienced the lowest wear rates at elevated temperatures, which was even lower than at room temperature.

**Keywords:** Sliding wear; Thermal spray coatings; $Cr_3C_2$; HVOF; HVAF.

*Corresponding author: Ville Matikainen (ville.matikainen@tut.fi)

## 1. INTRODUCTION

Surface engineering provides a wide range of techniques that can be used to alter the component surface in order to remarkably improve its performance, e.g. wear and corrosion resistance [1]. Thermal spraying belongs to these techniques and consists of coating processes that are capable of applying thick material layers on large surfaces [2]. Currently, high velocity oxygen-fuel (HVOF) sprayed hard metal coatings are the industrial standard solution for wear protection of components.

Hard metals are known for their wear resistance and the most common compositions used in thermal spraying are WC-Co/Ni with optional Cr addition and $Cr_3C_2$-NiCr [3]. The WC-based coatings are hard and provide good wear resistance compared to electroplated hard chromium [4,5]. However, their use at high temperatures (over 500 ºC) is limited by the low oxidation resistance of the hard WC particles embedded in the ductile metal matrix [6,7]. The $Cr_3C_2$-25NiCr coatings have often lower wear resistance compared to the WC-based coatings [4,5,8] but significantly higher oxidation resistance [9]. Therefore, they are used as wear resistant coatings at high temperatures up to 800-900 °C [10].

Several commercial $Cr_3C_2$-based powder materials are available that are designed to provide improved corrosion or wear resistance compared to the standard $Cr_3C_2$-25NiCr composition. The corrosion resistance can be improved closer to that of the metallic materials by increasing the metallic matrix content and by tailoring its composition, e.g. $Cr_3C_2$-50NiCrMoNb, while providing also good wear resistance [11]. On the other hand, the wear resistance of typical $Cr_3C_2$-25NiCr coatings can be improved by replacing some of the $Cr_3C_2$ particles with harder WC particles, e.g. $Cr_3C_2$-37WC-18NiCoCr [12].

The sliding wear behaviour of HVOF sprayed $Cr_3C_2$-25NiCr coatings has been studied at room temperature [8,13–15] and at elevated temperatures [8,16–18]. However, the performance of the alternative compositions has not been investigated and a comparative study is therefore needed to provide understanding about the room temperature and high temperature performance of these coatings.

As the deposition technique significantly affects the coating structure, it is of high interest to compare also the most viable spray processes used to produce the hard metal coatings, namely high velocity oxygen-fuel (HVOF) and high velocity air-fuel (HVAF) flame spray processes. The good properties of the coatings produced with the HVOF spray process are due to the high temperature supersonic gas stream which heats up and accelerates the powder particles to high velocities (500-800 m/s) and produces dense coatings [19]. However, some of the drawbacks especially of the gas fuelled HVOF process are related to the deposition rate and overheating of the finer particles, which causes carbide dissolution and brittle phase formation that in conjunction with tensile residual stresses can result in crack formation [20,21]. In the HVAF spray process the combustion takes place between gaseous fuel and compressed air instead of pure oxygen [22]. This dramatically decreases the flame temperature below 2000 °C [23,24] while producing even higher particle velocities compared to HVOF, over 900 m/s [25,26]. As a result, the coatings are denser and less oxidised, and finer particle size distributions can be used [27]. Several studies on long-term microstructural development and high temperature erosion have been carried out on $Cr_3C_2$-25NiCr coatings sprayed with the older HVAF torches [28–30]. The early HVAF torches used kerosene as the fuel and suffered from low particle temperature and deposition efficiency. The ease of operation and the deposition efficiency were significantly improved by later developments of the combustion chamber design allowing for the effective burning of gaseous fuels [22]. The research on coatings sprayed with the modern gaseous fuel HVAF torches has mostly focused on WC-based materials [21,31–33] and only recently studies on $Cr_3C_2$-based coatings have emerged [8,26,27,34].

This study compares the sliding wear behaviour of commercially available $Cr_3C_2$-25NiCr, $Cr_3C_2$-50NiCrMoNb and $Cr_3C_2$-37WC-18NiCoCr materials sprayed with HVOF and HVAF spray processes. The performance is assessed with a ball-on-disk test at room temperature and at 700 °C against an $Al_2O_3$ counterpart.

## 2. EXPERIMENTAL

### 2.1 Coating Materials

Commercial agglomerated and sintered $Cr_3C_2$-37WC-18M (M=NiCoCrFe) and $Cr_3C_2$-50NiCrMoNb powders were selected as interesting alternatives to conventional $Cr_3C_2$-25NiCr. In addition, two powders with the $Cr_3C_2$-25NiCr composition were chosen as reference materials. One of the $Cr_3C_2$-25NiCr materials was a common agglomerated and sintered powder whereas the other one was plasma densified after the agglomeration and sintering process (marked with (d)). Two particle size distributions were chosen for each of the four powders, which are hereafter designated as $-d_{90}+d_{10}$ [µm]. Finer particle size (-30+5 or -30+10 µm) was used with HVAF spraying and the coarser one (-38+10 µm or -45+15 µm) with HVOF spraying. The details of the powders are listed in **Table 1**.

***Table 1**: Details of the powders, processes and nominal particle size distribution given by manufacturer.*

| Powder composition | Manufacturing process | Spray process | Particle size (µm) | Manufacturer |
|---|---|---|---|---|
| $Cr_3C_2$-50NiCrMoNb | A&S | HVOF | -45+15 | H.C. Starck |
| $Cr_3C_2$-50NiCrMoNb | A&S | HVAF | -30+5 | H.C. Starck |
| $Cr_3C_2$-25NiCr | A&S | HVOF | -38+10 | H.C. Starck |
| $Cr_3C_2$-25NiCr | A&S | HVAF | -30+5 | H.C. Starck |
| $Cr_3C_2$-25NiCr (d) | A&S, densified | HVOF | -45+15 | Oerlikon Metco |
| $Cr_3C_2$-25NiCr (d) | A&S, densified | HVAF | -30+10 | Oerlikon Metco |
| $Cr_3C_2$-37WC-18NiCoCr | A&S | HVOF | -45+15 | Oerlikon Metco |
| $Cr_3C_2$-37WC-18NiCoCr | A&S | HVAF | -30+10 | Oerlikon Metco |

A&S = Agglomerated and sintered, (d) = densified

### 2.2 Spray Processing

Coatings were produced with commercial HVOF and HVAF guns, Diamond Jet Hybrid 2700 (Oerlikon Metco, Wohlen, Switzerland) and M3 (Uniquecoat Technologies LLC, Oilville, USA), respectively. The spray parameters are given in **Table 2**. Standard spray parameters were used for the HVOF spray process, while the HVAF spray parameters were selected based on preliminary tests aiming to provide high heating of the fine particles without creating coating defects. The flows of the process gases in the HVAF spray process are

pressure-controlled and therefore given in bar, while the gas flow rates for HVOF are given in slpm. The M3 HVAF spray process uses two propane injections designated here as *Propane 1* and *Propane 2*. Propane 1 is premixed with air and injected into the combustion chamber for the primary combustion, whereas Propane 2 is injected into the secondary extension nozzle with additional air [35]. Coatings were sprayed on 5 mm-thick low carbon steel substrates (S235) measuring 200x50 mm and the substrates were grit-blasted prior to spraying with mesh 36 alumina grit. A long combustion chamber, 4L2 nozzle and long powder injector were used as the hardware for HVAF spraying and propane as the fuel gas. Target coating thickness was 300 µm.

***Table 2:*** *Spray parameters used in HVAF and HVOF processes.*

| Parameter | HVAF | HVOF |
|---|---|---|
| Oxygen | - | 240 slpm |
| Air | 7.4 bar | 383 slpm |
| Propane 1 | 7.0 bar | 70 slpm |
| Propane 2 | 7.3 bar | - |
| Nozzle length | 255 mm | 95 mm |
| Spray distance | 300 mm | 230 mm |
| Surface speed | 1.9 m/s | 0.8 m/s |
| Pass spacing | 4 mm | 5.4 mm |
| Powder feed rate | 130-200 g/min | 60 g/min |

## 2.3 Sliding Wear

Sliding wear tests were performed with a ball-on-disk configuration on a high temperature tribometer (Anton-Paar Tritec, Peseux, Switzerland). The 23 x 23 $mm^2$ sized samples were ground and polished to obtain a surface roughness of Ra ≈ 0.02 µm. The polished samples were ultrasonically cleaned in acetone and mounted onto the rotating disk of the tribometer. Tests were performed both at room temperature and at 700 °C; in the latter case, the entire test area was enclosed in a refractory casing. The coated sample disk was induction heated to 700 °C and the temperature was monitored with a thermocouple in contact with the sample. Alumina sphere counterpart with 6 mm diameter was pressed on polished coating surfaces with 10 N normal load. The relative sliding speed was set to 0.10 m/s and wear track radius to 5 mm for room temperature tests and 7 mm for high temperature tests. A total sliding distance of 5000 m was used. The coefficient of friction was monitored during the test by using a load cell. The volume losses of the samples were measured by using an optical confocal profilometer (CHR150, Stil, Aix en Provence, France) and the ball wear was inspected with an optical microscope. Volume losses were converted to wear rates by normalizing over the sliding distance and normal load.

## 2.4 Characterisation

Metallographic samples of the as-sprayed coatings were prepared by mounting the cut section of the coating in resin and by grinding the samples with P220, P600 and P1200 SiC papers and polishing subsequently with 3 µm and 1 µm diamond suspensions. Final polishing was carried out with submicron colloidal silica. Cross sections of the as-sprayed coatings were analysed with scanning electron microscope (SEM: XL-30, Philips, Netherlands) by using the backscattered electron (BSE) detector. Porosity, carbide and matrix content were determined by image analysis with ImageJ [36] from ten SEM micrographs per coating. In addition, the areas of the carbides were determined from the SEM images and a diameter of a circle corresponding the measured surface area of each carbide was calculated. A mean carbide diameter (d50) was calculated from the resulting volume distribution of the analysed carbides.

The surfaces and cross sections of the wear scars were inspected with a field emission gun-scanning electron microscope (FEG-SEM: Nova NanoSEM 450, FEI, Eindhoven, Netherlands). The cross section samples after wear testing were prepared by cold mounting the specimen in epoxy resin prior to cutting to preserve the damaged wear surface. After cutting, the samples were ground and polished with diamond pads (up to P1200), 3 µm diamond suspension and submicron colloidal silica.

Moreover, micro-Raman spectroscopy (LabRam, Horiba Jobin-Yvon, Villeneuve D'Ascq, France) was employed to characterise the structure of the wear debris sticking to the wear tracks and of the oxide scale formed outside the wear track after testing at 700 °C. The laser radiation with a wavelength of 632.81 nm was

focused onto the samples using a 100x-magnification objective, achieving a lateral resolution of few micrometres and a penetration depth of some tens of nanometres [37].Loose wear debris was further analysed with a transmission electron microscope (TEM: JEM2010, Jeol, Tokyo, Japan), equipped with an EDX microanalysis detector.

Microhardness measurements were carried out on the cross sections of the coatings, both in the as-sprayed condition and after the high temperature tests, with an MMT-X7 Vickers microindenter (Matsuzawa, Akita, Japan) by using 0.3 kg load and 10 s dwell time to calculate an average hardness value from ten indentations.

## 3. RESULTS AND DISCUSSION

### 3.1. Coating characterisation

The microstructures of the as-sprayed coating cross sections in **Figure 1** show distinctive differences between the material compositions and between the two spray processes. When comparing the HVOF (top row) and HVAF (bottom row) sprayed coatings, it becomes clear that the higher processing temperature of HVOF spraying results in significant carbide dissolution and in some cases even complete melting of the carbides. This is seen as numerous dark stripes in the coating structure, especially well visible in the HVOF sprayed $Cr_3C_2$-50NiCrMoNb coating in **Figure 1a** (pointed by arrows). The $Cr_3C_2$-50NiCrMoNb (a-b) and $Cr_3C_2$-25NiCr (c-d) coatings in **Figure 1** both represent very similar structures consisting of dark carbide particles surrounded by metal matrix. Some small white spots are visible in the metal matrix of $Cr_3C_2$-50NiCrMoNb coatings, which were confirmed to be NbC precipitates by the XRD patterns in **Figure 2a**.

Compared to the agglomerated and sintered feedstock material, the HVOF sprayed coating from the densified $Cr_3C_2$-25NiCr powder shows some local large and grey matrix areas indicating significant carbide dissolution and increase in carbon content of the matrix (pointed by arrows in **Figure 1e**). This is promoted by the finer carbide size present in the feedstock material and in the resulting as-sprayed coating. Many of the densified particles indeed contain fine carbide structures, which are transferred into the as-sprayed coating structures (particularly in the HVAF-sprayed one) in **Figure 1e-f**. The formed coatings have seemingly high carbide content compared to the coatings in **Figure 1a-d**.

The XRD patterns also confirm the significant presence of $Cr_7C_3$ carbides in all coatings except for the HVAF sprayed $Cr_3C_2$-25NiCr one. Formation of $Cr_7C_3$ is often accompanied by the substitution of Cr in the carbides, e.g. by Ni to create $(Cr,Ni)_7C_3$ carbides [38]. Such changes increase the molecular weight of the structure, which shows in the BSE images as lighter grey carbides, e.g. in **Figure 1a-c** and **Figure 1e-f**. The HVAF sprayed $Cr_3C_2$-25NiCr coating microstructure in **Figure 1d** and the XRD pattern in **Figure 2b** contain only $Cr_3C_2$-type carbides with limited dissolution and increase in matrix carbon content due to lower combustion temperature. Some matrix areas in the coating structure represent minimal increase in carbon content, which leaves them brighter than the surrounding matrix in the BSE image due to higher molecular weight (arrows in **Figure 1d**). Another interesting feature can be detected in the XRD patterns of the plasma densified powder and the as-sprayed coatings; namely, they contain metastable $Cr_3C_{2-x}$ ($0 \leq x \leq 0.5$), presumably resulting from the powder manufacturing process [39].

The $Cr_3C_2$-37WC-18NiCoCrFe structures in **Figure 1g-h** contained homogeneously dispersed WC particles surrounded by darker and larger $Cr_3C_2$ particles and the light grey metal matrix. The WC particles are seen in the SEM images as blocky white particles and in the XRD patterns as high intensity peaks of WC.

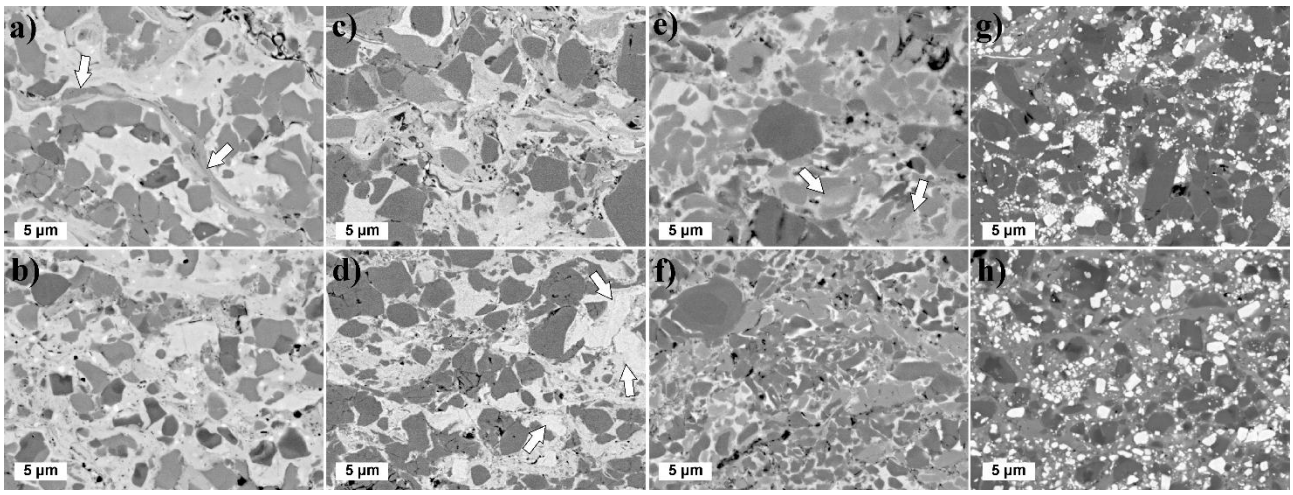


***Figure 1:*** *Detailed SEM images (BSE) of the cross section microstructures of HVOF (top row) and HVAF (bottom row) sprayed coatings of a-b) $Cr_3C_2$-50NiCrMoNb, c-d) $Cr_3C_2$-25NiCr, e-f) $Cr_3C_2$-25NiCr, plasma-densified, and g-h) $Cr_3C_2$-37WC-18NiCoCr.*

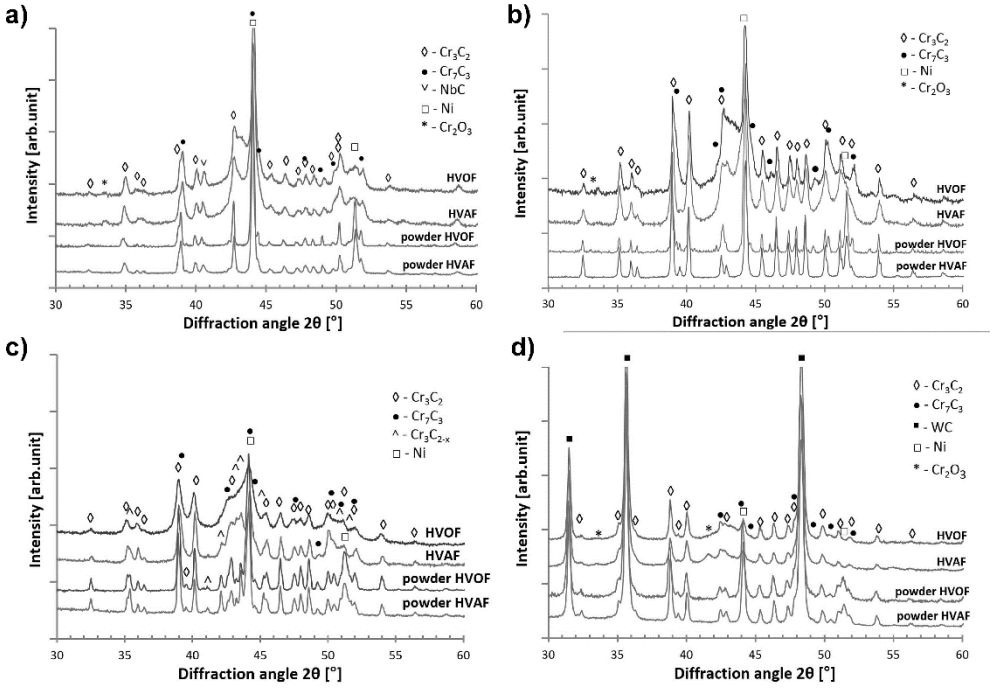


***Figure 2:*** *XRD patterns of the feedstock powders and as-sprayed coatings of a) $Cr_3C_2$-50NiCrMoNb, b) $Cr_3C_2$-25NiCr, c) $Cr_3C_2$-25NiCr (densified) and d) $Cr_3C_2$-37WC-18NiCoCr.*

The coating microstructures in **Figure 1** seemed to contain varying amounts of porosity and this was further confirmed by the image analysis results in **Table 3**. In general, the HVAF sprayed coatings contained lower amounts of porosity and were denser than the HVOF sprayed coatings. This was also supported by the open circuit potential tests in our previous study [27], confirming the significant reduction of open porosity. This results from the high particle velocities produced by the HVAF spray process when convergent-divergent 4L2 nozzle is used [35]. Lowest porosities were determined for the $Cr_3C_2$-50NiCrMoNb coatings with high matrix content and the $Cr_3C_2$-37WC-18NiCoCr coatings with the WC addition. One important factor decreasing the porosity of these coatings could be the higher material density, i.e. kinetic energy, compared to the other two compositions with higher $Cr_3C_2$ content. An additional factor can be the improved deformability of the $Cr_3C_2$-50NiCrMoNb particles due to the higher metallic matrix content. The highest porosity, on the other hand, was measured for the HVOF sprayed $Cr_3C_2$-25NiCr (d) coating, which shows many of the pores in conjunction with carbides in **Figure 1e**.

The coating microstructure and carbide content can be expected to play an important role in sliding wear. For this reason, the main structural components, namely carbide and matrix content, were determined by image

analysis from the coating cross sections. Mean carbide sizes were also determined for all coatings. The results in **Table 3** confirm that the $Cr_3C_2$-50NiCrMoNb coatings contain the lowest volume percentage of carbides. They are followed by the conventional $Cr_3C_2$-25NiCr coatings with approximately 55 vol% of carbides, which is significantly lower than the nominal 80 vol%. This may be ascribed to the rebounding of coarse carbide particles, in accordance with prior literature works [40]. The coatings sprayed from the densified $Cr_3C_2$-25NiCr powder are closer to the nominal carbide content, supposedly due to the finer measured carbide size, which is also visible in **Figure 1e-f**. The carbide content of the $Cr_3C_2$-37WC-18NiCoCr coatings again indicate loss of carbides especially when the HVAF spray process is used. The image analysis results indicate that significant carbide loss had taken place via dissolution and carbide rebounding during the spraying [40] with both processes. While the dissolution can be expected to be more significant with the HVOF spray process due to the higher process temperature supported by the before mentioned microstructural evidence of higher carbide dissolution, rebounding is probably responsible for most of the carbide loss in HVAF sprayed coatings, where much less evidence of dissolution exists.

The microhardness values in **Table 3** were lower for the $Cr_3C_2$-50NiCrMoNb with the lowest carbide content and higher for the HVAF sprayed $Cr_3C_2$-37WC-18NiCoCr. All $Cr_3C_2$-25NiCr coatings demonstrated similar hardness values of approximately 950 $HV_{0.3}$. The HVOF sprayed coatings showed consistently higher standard deviations of the measured values, which indicates more heterogeneous structure with significant variation in the local mechanical properties. This is caused by the variation in the heating of the particles when HVOF spray process is used. The high process temperature is causing significant carbide dissolution in the finer particles, which then create local carbon-saturated matrix areas with decreased carbide content. The variation in the individual hardness values was especially high for the HVOF sprayed $Cr_3C_2$-37WC-18NiCoCr coating compared to the HVAF sprayed counterpart.

***Table 3:*** *Measured porosity, chromium carbide, matrix, tungsten carbide content and microhardness, as well as determined $Cr_3C_2$ and WC carbide sizes for all the sprayed coatings.*

| | | **Porosity [vol%]** | **$Cr_3C_2$ [vol%]** | **Matrix [vol%]** | **WC [vol%]** | **$Cr_3C_2$ / WC size [µm]** | **Hardness [$HV_{0.3}$]** |
|---|---|---|---|---|---|---|---|
| $Cr_3C_2$-50NiCrMoNb | HVOF | 0.8 (±0.3) | 44.5 (±3.5) | 54.7 (±3.4) | | 2.4 | 806 (±117) |
| $Cr_3C_2$-50NiCrMoNb | HVAF | 0.5 (±0.3) | 44.9 (±3.9) | 54.6 (±3.9) | | 2.1 | 885 (±58) |
| $Cr_3C_2$-25NiCr | HVOF | 1.7 (±1.0) | 54.7 (±4.8) | 43.6 (±5.2) | | 2.5 | 938 (±79) |
| $Cr_3C_2$-25NiCr | HVAF | 1.5 (±0.5) | 55.1 (±3.2) | 43.5 (±3.3) | | 2.1 | 920 (±51) |
| $Cr_3C_2$-25NiCr (d) | HVOF | 2.2 (±0.4) | 61.1 (±4.8) | 36.7 (±4.7) | | 2.2 | 947 (±144) |
| $Cr_3C_2$-25NiCr (d) | HVAF | 1.0 (±0.7) | 70.1 (±3.7) | 28.8 (±3.7) | | 1.6 | 958 (±69) |
| $Cr_3C_2$-37WC-18NiCoCr | HVOF | 0.5 (±0.2) | 45.9 (±4.7) | 37.7 (±4.8) | 15.9 (±2.2) | 1.6 / 0.7 | 934 (±195) |
| $Cr_3C_2$-37WC-18NiCoCr | HVAF | 0.6 (±0.2) | 32.4 (±3.1) | 46.6 (±3.4) | 20.3 (±1.4) | 1.5 / 0.7 | 1104 (±118) |

## 3.2. Sliding Wear at Room Temperature

### 3.2.1. Wear Rate and Coefficient of Friction

The friction curves recorded on all coatings exhibit an initial running-in stage with increasing friction coefficient and a subsequent steady-state regime, which lasts for most of the test duration. All samples but the HVOF and HVAF sprayed $Cr_3C_2$-25NiCr (d) coatings from plasma densified powder attain the steady state within the initial 500 m. Steady state coefficients of friction are comprised in a relatively narrow range between 0.64 and 0.78, as summarised in **Table 4**. Such narrow range indicates a small effect of the spray process and the composition on the steady-state coefficient of friction.

Interestingly, the HVOF and HVAF sprayed $Cr_3C_2$-25NiCr (d) coatings exhibit an extended running-in regime, a less stable friction coefficient in the steady-state regime (**Figure 3**), and experience significantly higher wear rates compared to the other coatings: $8.14*10^{-6}$ $mm^3/(Nm)$ for the HVOF sprayed coating and $9.74*10^{-6}$ $mm^3/(Nm)$ for the HVAF sprayed one. The $Al_2O_3$ counterpart did not experience measurable material loss during the testing of the $Cr_3C_2$-25NiCr (d) coatings.

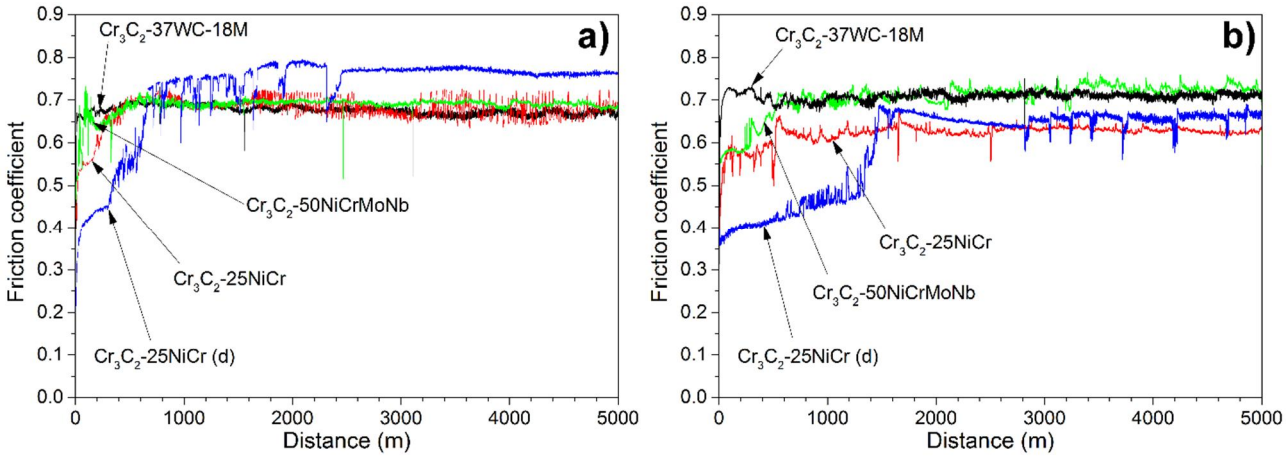


***Figure 3**: evolution of the friction coefficient during room temperature ball-on-disk testing of HVOF (a) and HVAF (b) sprayed coatings.*

The HVOF and HVAF sprayed coatings from the agglomerated and sintered $Cr_3C_2$-25NiCr powder experienced significantly lower wear rates of $1.58*10^{-6}$ $mm^3/(Nm)$ and $1.77*10^{-6}$ $mm^3/(Nm)$, respectively. Slightly higher wear rates of 2.18-2.19 $*10^{-6}$ $mm^3/(Nm)$ were measured for the $Cr_3C_2$-50NiCrMoNb coatings. The higher wear rate compared to the $Cr_3C_2$-25NiCr coatings is likely due to the higher matrix content of the coatings. However, the difference in wear rate between the coatings from agglomerated and sintered $Cr_3C_2$-25NiCr and $Cr_3C_2$-50NiCrMoNb powders is very small when considering the difference in matrix content and coating hardness, e.g. HVOF sprayed $Cr_3C_2$-50NiCrMoNb with 806 $HV_{0.3}$ microhardness compared to the HVOF sprayed $Cr_3C_2$-25NiCr coating with 938 $HV_{0.3}$.

The lowest coating wear rates were measured for the $Cr_3C_2$-37WC-18NiCoCr coatings with additional WC hard particles. The wear rate of the HVAF sprayed coating, 0.38 $*10^{-6}$ $mm^3/(Nm)$, was approximately one fifth of the wear rate of the common $Cr_3C_2$-25NiCr coatings. However, the ball wear rate was significantly higher in the case of the HVOF sprayed $Cr_3C_2$-37WC-18NiCoCr coating which is probably promoted by the coarse surface with protruding WC particles. Similar behaviour between HVAF and HVOF sprayed $Cr_3C_2$-37WC-18NiCoCr coatings was observed by Hulka et al. when using WC-Co ball as the counterpart [12]. They also found that the ball wear rate was significantly higher in the case of the HVOF sprayed coating. The reason for this could be the potentially coarser wear debris size arising from the brittle cracking of the coating surface or the higher carbide content compared to the HVAF sprayed coating. The $Cr_3C_2$-37WC-18NiCoCr coatings exhibited higher wear rates compared to the HVOF and HVAF sprayed WC-10Co4Cr coatings tested with the same parameters by Bolelli et al. in [7,21]. The WC-10Co4Cr coatings experienced wear rates of 2-8$*10^{-8}$ $mm^3/(Nm)$, which highlights the effect of the material composition. Similarly improved wear resistance was observed on the WC-$(W,Cr)_2C$-Ni coating with $1.5*10^{-7}$ $mm^3/(Nm)$ wear rate in [7].

***Table 4:** Coefficients of friction, wear rates and hardness values of the tested coatings at room temperature. Standard deviation is given inside the brackets.*

| Powder composition | Spray process | Wear rate [$*10^{-6}$ $mm^3/(Nm)$] | Ball wear rate [$*10^{-8}$ $mm^3/(Nm)$] | Coefficient of Friction |
|---|---|---|---|---|
| $Cr_3C_2$-50NiCrMoNb | HVOF | 2.18 (±0.38) | 9.73 (±1.10) | 0.68 (±0.01) |
| $Cr_3C_2$-50NiCrMoNb | HVAF | 2.19 (±0.02) | 3.06 (±1.36) | 0.71 (±0.01) |
| $Cr_3C_2$-25NiCr | HVOF | 1.58 (±0.75) | 2.41 (±0.86) | 0.68 (±0.00) |
| $Cr_3C_2$-25NiCr | HVAF | 1.77 (±0.04) | 6.81 (±0.44) | 0.64 (±0.03) |
| $Cr_3C_2$-25NiCr (d) | HVOF | 8.14 (±1.05) | 0 | 0.78 (±0.01) |
| $Cr_3C_2$-25NiCr (d) | HVAF | 9.74 (±4.69) | 0 | 0.70 (±0.06) |
| $Cr_3C_2$-37WC-18NiCoCr | HVOF | 0.63 (±0.04) | 21.80 (±10.81) | 0.69 (±0.02) |
| $Cr_3C_2$-37WC-18NiCoCr | HVAF | 0.38 (±0.06) | 8.43 (±2.24) | 0.71 (±0.00) |

### 3.2.2. Wear mechanism

At room temperature, the wear mechanism was similar for all coatings. In all cases, wear depended on a combination of i) abrasive grooving, ii) brittle fracture, iii) delamination and iv) tribo-oxidation [8].

*Abrasive grooving* can be seen on all of the wear tracks presented in **Figure 4**. The grooving and resulting material removal was less obvious in the case of the $Cr_3C_2$-37WC-18NiCoCr in **Figure 4g-h**, where the protruding harder WC particles decreased the wear of the surrounding coating surface. These protruding particles created shadowed areas behind them, preventing the material removal. For instance, in **Figure 4h**, the arrows point out to some abrasive grooves which, starting from the edges of a cluster of hard, protruding WC particles, cross a large chromium carbide-based area; immediately behind the WC particles, on the other hand, no grooves are seen due to the mentioned shadowing effect. The higher resistance to grooving resulted in the lowest wear rates among the tested coatings.

*Brittle fracture*, caused by the cyclic stresses of the wear test, led to pull-outs of material from the sample surfaces. The created cavities, which were often filled with wear debris, can be seen on HVOF sprayed $Cr_3C_2$-25NiCr (d) coating in **Figure 4e** (arrows).Material removal by brittle cracking was particularly noticeable on both $Cr_3C_2$-25NiCr (d) coatings. This cracking eventually led to *the delamination* of the topmost layers of the coating, e.g. on the HVAF sprayed coating in **Figure 4f** (circled area). Such aggressive material removal increased the wear rates of both HVOF and HVAF sprayed coatings. Repeated delamination events are also the most likely explanation for the greater instability of the steady-state friction coefficient of these samples, as noted in Section 3.2.1 and **Figure 3**. The delamination phenomena of the $Cr_3C_2$-25NiCr (d) coatings could be linked to the significantly higher measured carbide content (see Section 3.1). The high carbide content with smaller mean carbide size compared to $Cr_3C_2$-25NiCr coatings effectively reduced the carbide mean free path, i.e. amount of metallic matrix between the carbides. On the one hand, the smaller mean free path may help lowering the friction coefficient in the initial sliding stages (see the friction curves in **Figure 3**), as most of the contact is borne by the carbide particles. On the other hand, it embrittles the coating, favouring the onset of severe brittle fracture and delamination after enough sliding cycles have accumulated to trigger significant surface fatigue phenomena. In addition, reduced carbide size promotes the carbide dissolution during HVOF spraying due to the increased surface area, as mentioned in Section 3.1, which further embrittles the metallic matrix. Crack formation can also be noticed on the HVOF sprayed $Cr_3C_2$-37WC-18NiCoCr coating in **Figure 4g** (arrows), while such distinct cracks were not formed on the wear track of the HVAF sprayed coating in **Figure 4h**. Similar behaviour on the HVOF sprayed $Cr_3C_2$-37WC-18NiCoCr coating was observed in [12]. The susceptibility to cracking in the case of the two HVOF sprayed coatings is supported by the detected high standard deviation of the microhardness measurements in **Table 3**, indicating heterogeneous coating structure and possible presence of brittle areas in the coating caused by carbide dissolution.

*Tribo-oxidation* occurred as a result of the high contact pressure between the surface asperities or loose debris and the $Al_2O_3$ counterpart, which resulted in locally elevated temperature. This led to the formation of fine oxidised wear debris as well as smeared oxide clusters on the sample surfaces. An example of the smeared material can be seen on the surface of the HVAF sprayed $Cr_3C_2$-50NiCrMoNb coating in **Figure 4b**, where an area is covered by an oxide cluster. The presence of substantial amounts of oxygen in the smeared clusters is confirmed by EDX spectra (**Figure 5**). The clusters (**Figure 4b** and **Figure 5a,c,e**) often had a wave-like shape because of the smearing under high pressure between the coating and the $Al_2O_3$ ball surface. This morphology reveals the action of large tangential forces inducing out-of-plane shear stresses and, consequently, out-of-plane plastic flow. The smeared oxide clusters on the coating surfaces did not seem to have a significant effect on the coefficients of friction in **Table 4**. While the wear debris on sample surfaces consisted mostly of oxidised material clusters, also some rolled material and individual pull-out particles were observed, e.g. on the HVAF sprayed $Cr_3C_2$-25NiCr coating in **Figure 4d** (circles).

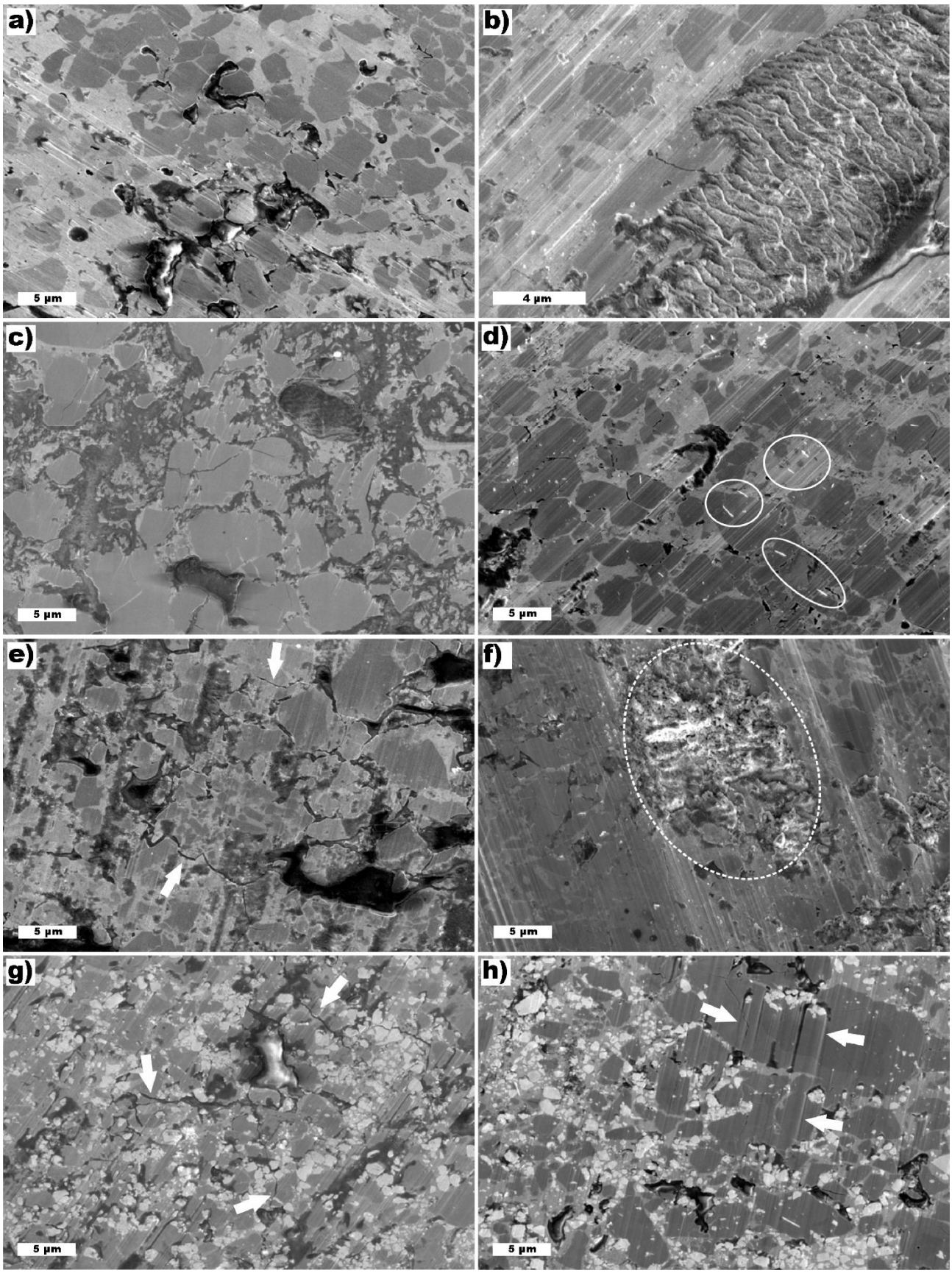


***Figure 4:*** *Detailed views of the wear tracks after testing a-b) the $Cr_3C_2$-25 NiCrMoNb coatings, c-d) the $Cr_3C_2$-25NiCr coatings, e-f) the $Cr_3C_2$-25NiCr (d) coatings and g-h) the $Cr_3C_2$-37WC-18NiCoCr coatings. The HVOF sprayed coatings are presented on the left side and HVAF sprayed coatings on the right side. Solid lined circle indicates wear debris, dashed line fractured area and arrows individual cracks or grooves.*

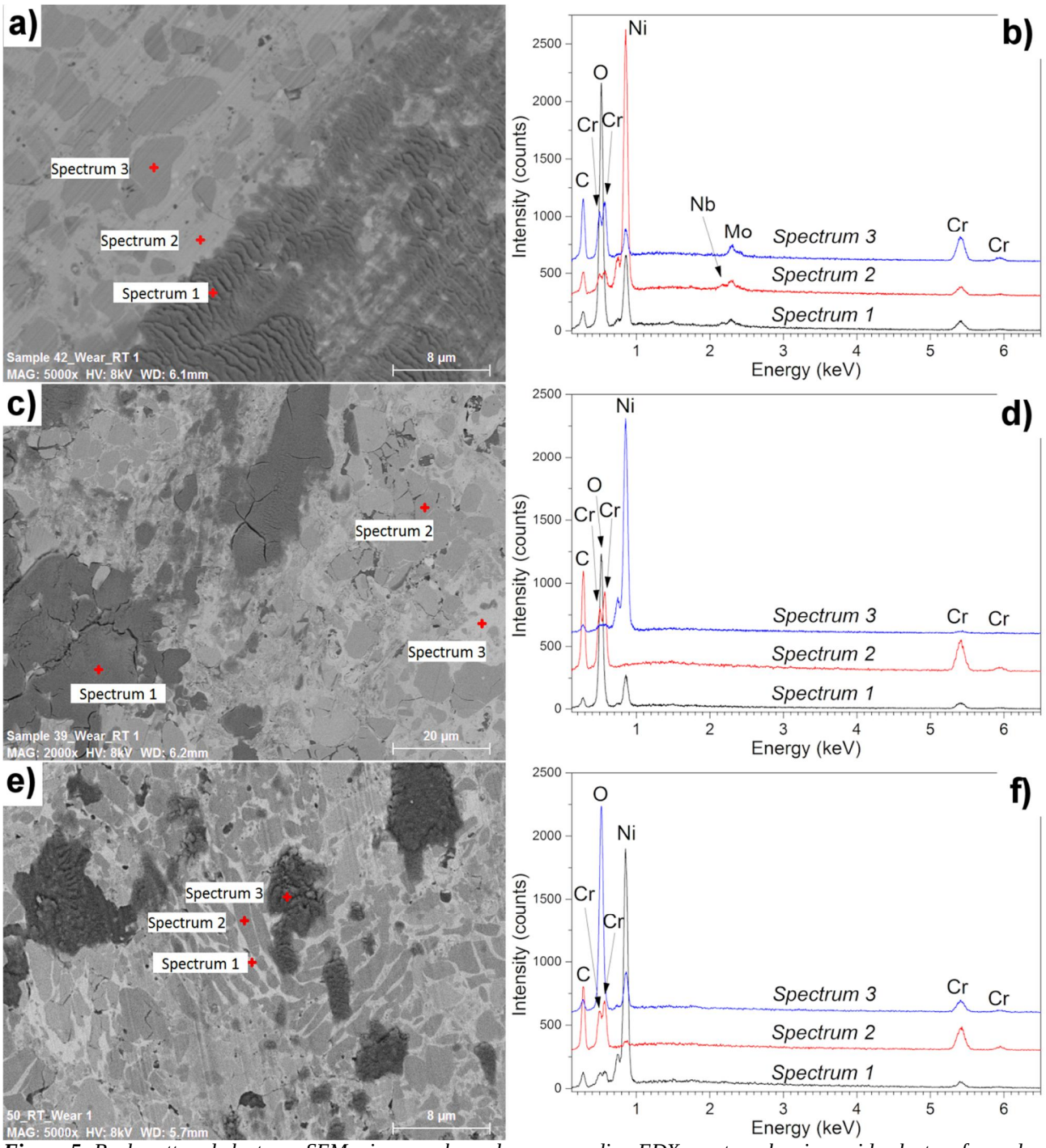


***Figure 5**: Backscattered electrons SEM micrographs and corresponding EDX spectra, showing oxide clusters formed on the worn surfaces of (a,b) HVAF-sprayed $Cr_3C_2$-50NiCrMoNb, (c,d) HVOF-sprayed $Cr_3C_2$-25NiCr and (e,f) HVAF-sprayed $Cr_3C_2$-NiCr, plasma-densified.*

Wear debris was collected from the wear surfaces after testing to further analyse the size, morphology and crystal structure of the debris with TEM. Fine particles and clusters of particles from HVOF sprayed $Cr_3C_2$-25NiCr (d) coating are seen in **Figure 6a**. The wear debris consisted of very fine particles with the size ranging from micrometric to nanometric. The high resolution TEM image of the particles in **Figure 6b** reveals a structure which is missing the crystalline features. This is confirmed by the amorphous halo and the faint diffraction spots visible in the selected area electron diffraction (SAED) pattern in **Figure 6c**.

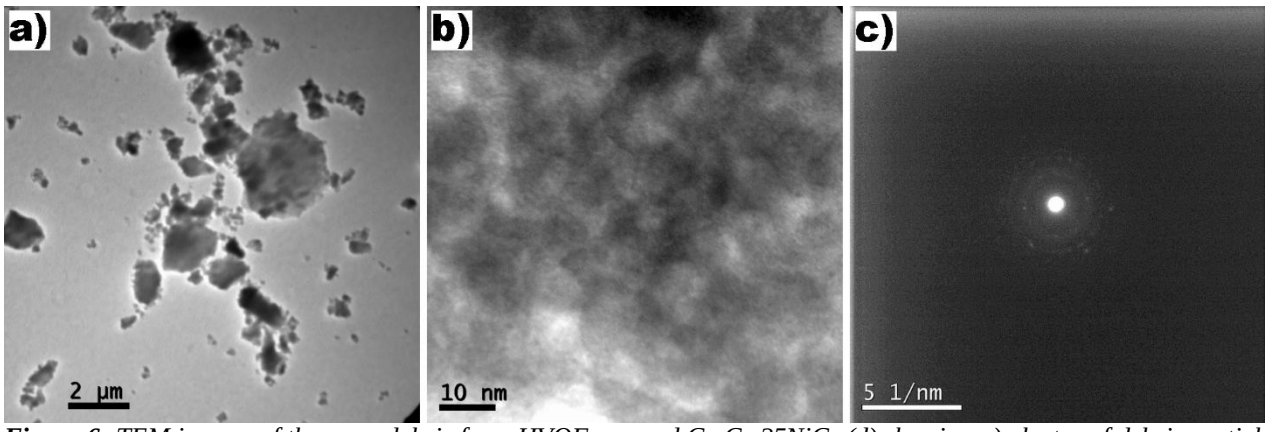


***Figure 6:*** *TEM images of the wear debris from HVOF sprayed $Cr_3C_2$-25NiCr (d) showing a) cluster of debris particles, b) poorly crystalline structure of the fine particles and c) the SAED pattern of the poorly crystalline debris.*

The debris clusters on the coating surfaces (such as those seen in **Figure 5**) were also analysed with Raman spectroscopy. The spectra in **Figure 7** were obtained from three separate clusters on the wear surfaces of HVOF sprayed $Cr_3C_2$-25NiCr, $Cr_3C_2$-50NiCrMoNb and $Cr_3C_2$-37WC-18NiCoCr coatings, respectively, and they confirm the TEM observations of the poorly crystalline structure of the wear debris. Specifically, the debris on $Cr_3C_2$-25NiCr coatings in **Figure 7a** features broad peaks in the 500 – 700 $cm^{-1}$ region, suggesting the formation of amorphous Cr- and Ni-based oxides and hydroxides [41]. Additional bands around 1360 $cm^{-1}$ and 1580 $cm^{-1}$ are ascribed to graphitic C [42], and may reflect the embedment of non-oxidised carbide fragments containing some excess C. This could come either from a pre-existing excess of C in the feedstock material or from some alteration of the debris fragments related to the partial oxidation of Cr. The debris clusters on $Cr_3C_2$-50NiCrMoNb coatings in **Figure 7b** accordingly exhibit bands in the 500 – 700 $cm^{-1}$ region, but the features at about 680 – 700 $cm^{-1}$ are slightly more pronounced than in **Figure 7a**, which may be ascribed to the formation of poorly crystalline spinel oxides such as $NiCr_2O_4$ [43]. Graphitic C is again detectable, revealing the presence of excess C as in the former case. In the $Cr_3C_2$-37WC-18NiCoCr coatings, broad peaks also occur at about 900 $cm^{-1}$ (**Figure 7c**), which may belong to $WO_3$ [44] and/or to tungstate compounds [45–47]. The peaks of graphitic C are again present, but the intensity is significantly lower.

A direct relation between the formation of amorphous, oxidised debris, as it has been inferred from TEM and Raman analyses, and high friction values, as listed in **Table 4**, has been postulated by Wesmann et al. [48]. Amorphous oxides, which lack any easy shear plane, do not exert a solid lubricant action. To the contrary, debris clusters on the coating surface may get stuck with similar clusters built up on the counterbody, which are seen in optical micrographs of the latter (**Figure 8**), also because of the presence of humidity in the environment. Accordingly, the $Cr_3C_2$-NiCr (d) coatings retain their low friction (**Figure 3**) until severe delamination phenomena (in accordance with the previous discussion on wear mechanisms) cause the rapid appearance of large amounts of debris. Sudden drops of friction during the steady-state regime in these coatings can similarly be ascribed to the fact that some delamination events can also result in the removal of the oxidised clusters responsible of high friction. Wesmann et al. [48] also detected free C in the debris, as in the present case (**Figure 7**), yet this is not effective to reduce friction either.

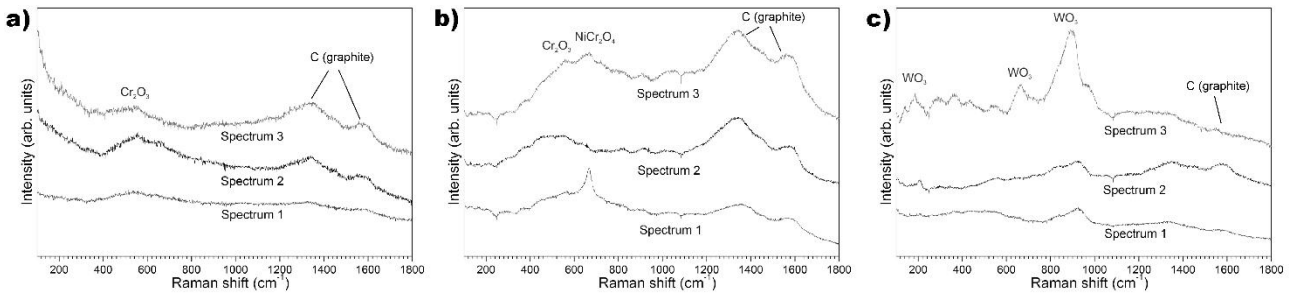


***Figure 7:*** *Raman spectra of the oxidised debris clusters on HVOF sprayed a) $Cr_3C_2$-25NiCr, b) $Cr_3C_2$-50NiCrMoNb and c) $Cr_3C_2$-37WC-18NiCoCr coatings.*

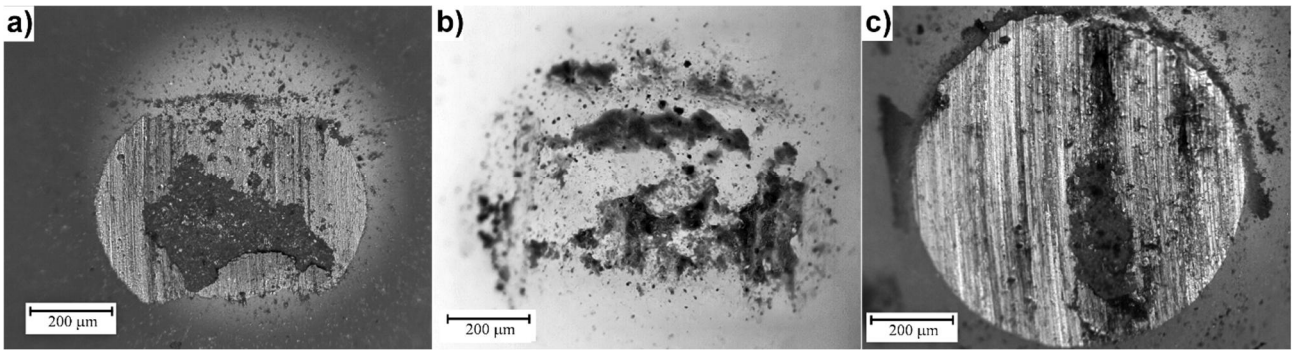

***Figure 8:*** *Optical micrographs of the worn $Al_2O_3$ surfaces after ball-on-disk wear testing at room temperature against HVOF-sprayed a) $Cr_3C_2$-25NiCr, b) $Cr_3C_2$-25NiCr, plasma-densified, and c) $Cr_3C_2$-37WC-18NiCoCr coatings.*

## 3.3. Sliding Wear at 700 °C

### 3.3.1. Wear Rate and Coefficient of Friction

The results from the high temperature sliding wear tests and coating hardness values after the tests are summarised in **Table 5**. The hardness measurements were performed on the cross sections similar to the as-sprayed coatings. The wear rate and coefficient of friction results differ significantly from those of the room temperature test (in **Table 4**). Firstly, the $Al_2O_3$ counterpart did not experience any measurable material loss during the high temperature tests. Secondly, the $Cr_3C_2$-50NiCrMoNb and $Cr_3C_2$-37WC-18NiCoCr coatings experienced increased wear rates compared to the room temperature results. By contrast, the coatings with $Cr_3C_2$-25NiCr chemical composition experienced mainly decreased wear rates at high temperature.

More specifically, the HVAF $Cr_3C_2$-25NiCr coating experienced the lowest wear rate of $0.68*10^{-6}$ $mm^3/(Nm)$. As a term of comparison, HVOF-sprayed WC-$(W,Cr)_2C$-Ni coatings tested under very similar conditions at 750 °C exhibited wear rates $\geq 4*10^{-6}$ $mm^3/(Nm)$ [7]. The HVOF $Cr_3C_2$-25NiCr and $Cr_3C_2$-25NiCr (d) coatings both reached the same wear rate of $\approx 3*10^{-6}$ $mm^3/(Nm)$, while higher standard deviation can be observed for the latter. The HVAF-sprayed $Cr_3C_2$-25NiCr (d) coating, on the other hand, experienced the highest wear rate from the group of $Cr_3C_2$-25NiCr coatings, with an average value of $5.9*10^{-6}$ $mm^3/(Nm)$.

The wear rates of both $Cr_3C_2$-50NiCrMoNb coatings were significantly higher than those of $Cr_3C_2$-25NiCr coatings, reaching $>10*10^{-6}$ $mm^3/(Nm)$. However, the wear rates are significantly lower than those measured for HVOF sprayed iron and nickel based metallic coatings at 700 °C [18]. Indeed, the measured wear rates for FeNiCrBSi and NiCrFeSiB coatings were approximately $4*10^{-4}$ $mm^3/(Nm)$ and $8*10^{-4}$ $mm^3/(Nm)$, respectively [18]. The performance of the $Cr_3C_2$-50NiCrMoNb coating is comparable to that of NiCrAlY+$Al_2O_3$ composites characterised in [49], which also experienced wear rates slightly higher than $10*10^{-6}$ $mm^3/(Nm)$ when tested at 700 °C under analogous ball-on-disk conditions.
The wear rates of both HVAF and HVOF $Cr_3C_2$-37WC-18NiCoCr coatings were comparable with the wear rates of the $Cr_3C_2$-50NiCrMoNb coatings.

Friction curves (**Figure 9**) are remarkably different from the room-temperature ones (**Figure 3**): at 700 °C, a steady-state regime characterised by a relatively low friction is readily attained very soon after the beginning of the test. The average steady-state coefficients of friction are presented in the **Table 5**. All $Cr_3C_2$-25NiCr coatings experienced values of ≈0.35, which are significantly lower than the values of 0.60-0.78 measured at room temperature in **Table 4** or of 0.65, reported in another study [18]. The $Cr_3C_2$-50NiCrMoNb coatings experienced slightly higher values of ≈0.4, while the HVOF $Cr_3C_2$-37WC-18NiCoCr coating reached the highest coefficient of friction, 0.48. The highest values are in the same range with those of the iron based metallic coatings tested previously by Bolelli et al. [18].

***Table 5**: Coefficients of friction and wear rates of the tested coatings at 700 °C. Hardness measurements were done after the tests at room temperature. Standard deviation is given inside the brackets.*

| Powder composition | Spray process | Wear rate [*10$^{-6}$ mm$^3$/(Nm)] | Coefficient of Friction | Hardness ($HV_{0.3}$) |
|---|---|---|---|---|
| $Cr_3C_2$-50NiCrMoNb | HVOF | 24.66 (±5.07) | 0.39 (±0.02) | 905 (±100) |
| $Cr_3C_2$-50NiCrMoNb | HVAF | 15.73 (±0.40) | 0.40 (±0.01) | 847 (±52) |
| $Cr_3C_2$-25NiCr | HVOF | 3.13 (±0.18) | 0.36 (±0.01) | 1000 (±83) |
| $Cr_3C_2$-25NiCr | HVAF | 0.68 (±0.02) | 0.37 (±0.06) | 838 (±49) |
| $Cr_3C_2$-25NiCr (d) | HVOF | 3.20 (±0.94) | 0.35 (±0.01) | 1188 (±99) |
| $Cr_3C_2$-25NiCr (d) | HVAF | 5.86 (±1.20) | 0.35 (±0.01) | 1003 (±71) |
| $Cr_3C_2$-37WC-18NiCoCr | HVOF | 23.79 (±5.86) | 0.48 (±0.01) | 1258 (±110) |
| $Cr_3C_2$-37WC-18NiCoCr | HVAF | 19.13 (±4.25) | 0.40 (±0.04) | 1275 (±92) |

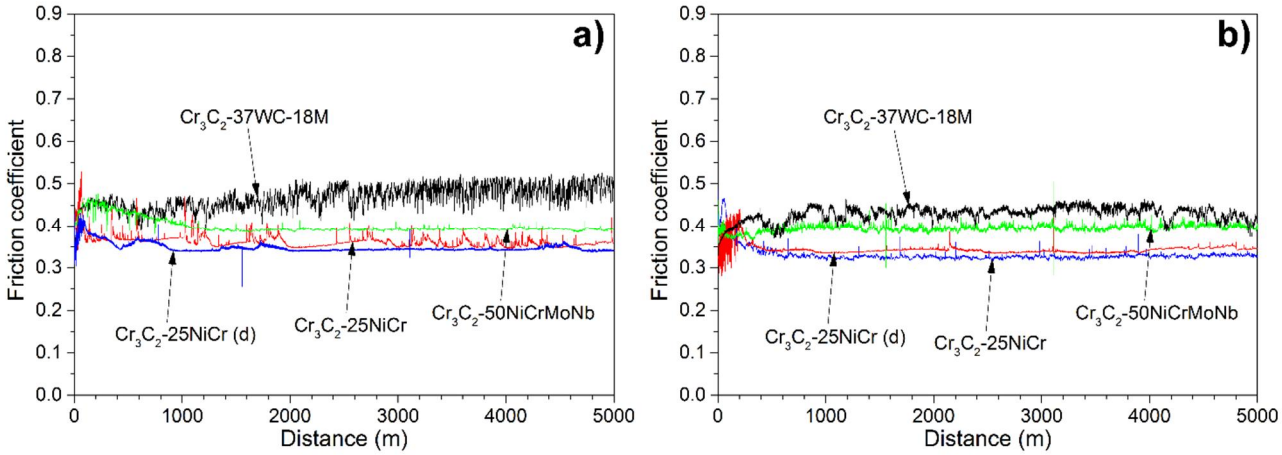


***Figure 9**: evolution of the friction coefficient during ball-on-disk testing of HVOF (a) and HVAF (b) sprayed coatings at 700 °C.*

### 3.3.2. Tribolayer and Wear Mechanism

The overall good wear resistance and low coefficient of friction values of the HVOF and HVAF sprayed $Cr_3C_2$-25NiCr coatings are a result of a tribo-oxidation wear regime shown in **Figure 10a**. Indeed, a smooth oxide-based tribolayer was formed on the wear track of the conventional $Cr_3C_2$-25NiCr coatings. The layer probably forms in the beginning of the test as a result of breaking and smearing of the oxide scale developed on the coating surface. Wear proceeds by a dynamic process, in which the smooth tribolayer breaks out in small flakes (delamination may occur within the tribolayer or within the underlying hardmetal as better detailed later on in Section 3.4.2.), exposing new coating surface to be oxidized. The partial breaking up of the tribolayer can be seen in **Figure 10b**, where small cracks have formed on the surface and parts of the layer are getting loose. The newly formed wear debris is then removed from the wear track or smeared on the exposed coating surface. The tribolayer is eventually reformed by the combination of smearing of the debris and oxidation of the exposed surface. Smooth smeared areas can be detected in **Figure 10c** with fine-grained material clusters around the edges. The formation of the smooth oxide layer on the sliding contact is clearly one of the benefits of chromium carbide based coatings compared to metallic coatings. The structure of the metallic coatings is softened and they experience high wear rates [18]. This softened structure does not provide sufficient support for the formation of a uniform oxide layer. The tribolayer and the supporting microstructure underneath protects the coating from the direct contact of the alumina ball.

The collected wear debris from the tested coating surfaces was further analysed with TEM. It can be observed from **Figure 11a** that the imaged debris cluster collected from HVOF sprayed $Cr_3C_2$-25NiCr coating consists of fine submicron particles. Contrary to the debris collected after the room temperature test, the high resolution image in **Figure 11b** shows the crystalline structure of the fine particles, confirmed by the SAED image in **Figure 11c**. Dynamic re-crystallisation of these highly deformed and comminuted debris particles is probably due to the high temperature of the system during the sliding wear test.

Whilst the amorphous debris clusters accumulating on the coating and on the counterbody at room temperature promoted high friction (Section 3.2.2), the smooth, crystalline oxide tribofilms (seen in **Figure 10**) are probably responsible for the low steady-state friction. Accordingly, friction spikes sometimes appearing during the steady-state regime (**Figure 9**) can be related to tribofilm delamination events (in accordance with the previous discussion on wear mechanisms), which briefly allow direct contact between the counterbody and the uncovered coating surface. It is also important to note that no oxide clusters formed on the counterbody surface (**Figure 12**), which only exhibits mild grooving without forming a flattened wear cap

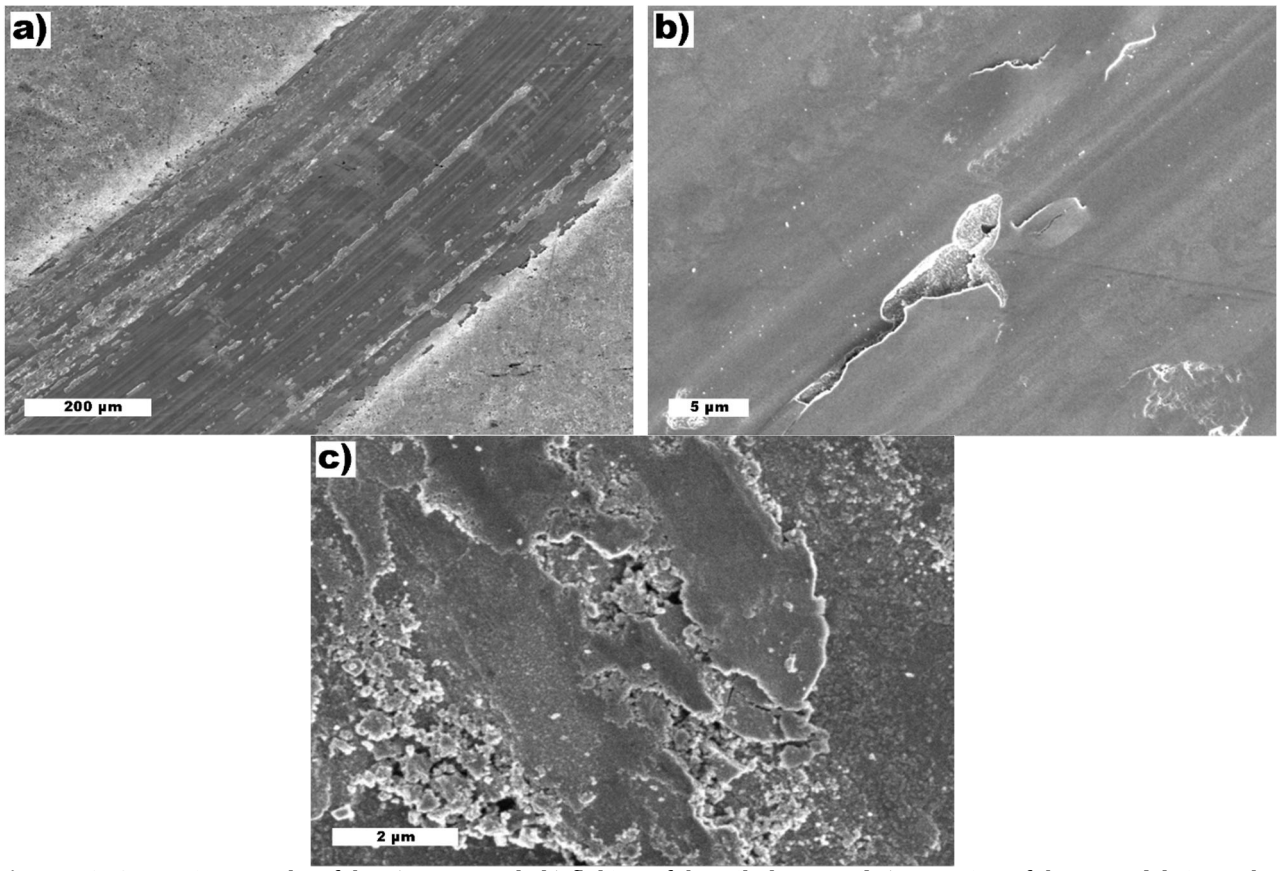


***Figure 10**: SEM micrographs of the a) wear track, b) flaking of the tribolayer and c) smearing of the wear debris on the surfaces of the wear scars obtained after ball-on-disk testing at 700 °C on HVOF-sprayed $Cr_3C_2$-25NiCr.*

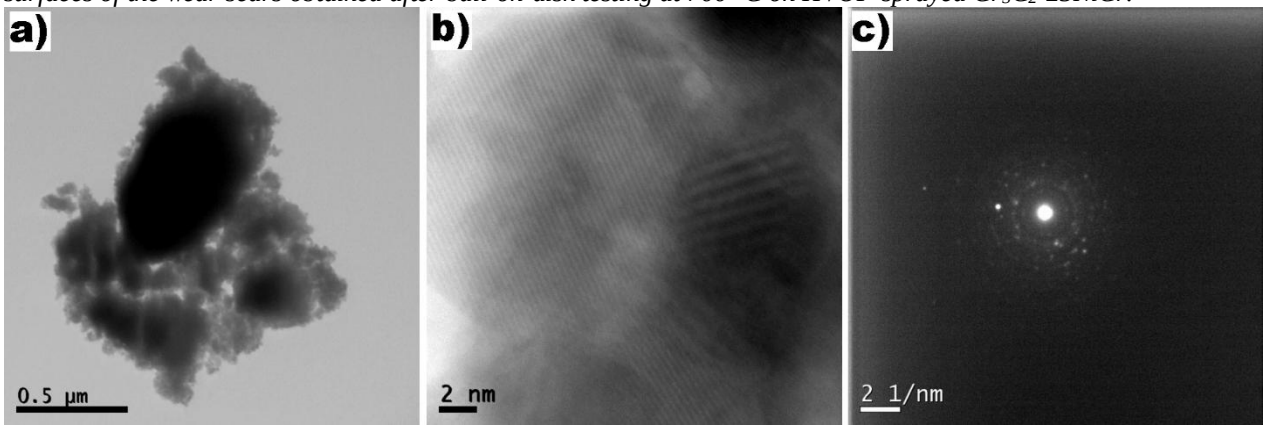


***Figure 11**: TEM images of the wear debris from HVOF sprayed $Cr_3C_2$-25NiCr coating showing a) cluster of debris particles, b) crystalline structure of the fine particles and c) the SAED pattern confirming the crystalline nature of the debris.*

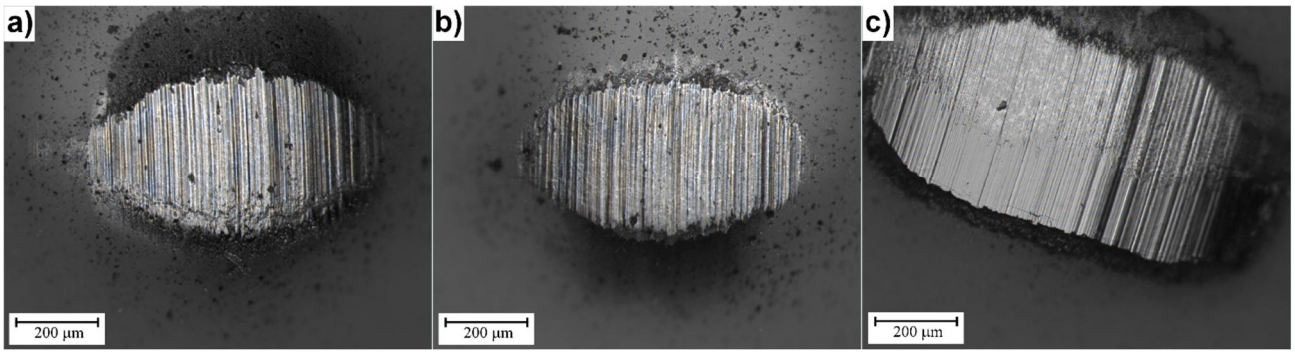


***Figure 12:*** *Optical micrographs of the worn $Al_2O_3$ surfaces after ball-on-disk wear testing at 700 °C against HVOF-sprayed a) $Cr_3C_2$-25NiCr, b) $Cr_3C_2$-25NiCr, plasma-densified, and c) $Cr_3C_2$-37WC-18NiCoCr coatings.*

The tribolayer formation was similar between the coatings sprayed from the conventional and the densified $Cr_3C_2$-25NiCr powders, but analysis of the wear surfaces showed significant difference in wear mechanisms. Both HVOF and HVAF $Cr_3C_2$-25NiCr (d) coatings were susceptible to large-scale delamination of the top surface layer and the tribolayer. The HVOF coating surface in **Figure 13a** shows large delaminated areas instead of the flaking and small-scale material removal observed in conventional $Cr_3C_2$-25NiCr coatings (**Figure 10b**). The detailed view of the cracking in **Figure 13b** suggests that the tribolayer is not strong enough or strongly enough attached to the underlying coating to withstand the continuous stress cycles, and in many cases, direct failure of the underlying hardmetal occurs, as better detailed in Section 3.4.2.

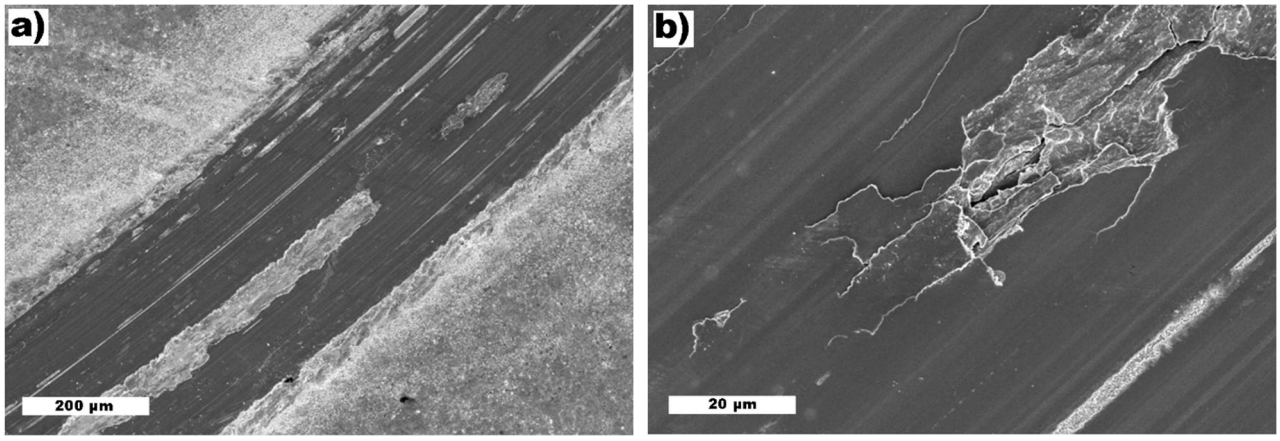


***Figure 13****: SEM image from HVOF sprayed $Cr_3C_2$-25NiCr (d) coating a) indicating the delaminated area (oval) on the wear track and b) more detailed view of the tribolayer delamination.*

The $Cr_3C_2$-50NiCrMoNb coatings experienced similar wear mechanisms as the coatings with $Cr_3C_2$-25NiCr composition. Uniform oxide layers were formed on the wear tracks of both coatings, which enabled the low coefficient of friction. However, the values were slightly higher than in the case of the $Cr_3C_2$-25NiCr coatings, which might have been caused by different oxide scale composition. Raman spectra were measured to study the compounds present in different locations of the tribolayer and in the oxide scales outside the wear track. The results of the analysis are presented in **Figure 14** and reveal that the tribolayer of the $Cr_3C_2$-50NiCrMoNb coatings mainly consisted of $NiCr_2O_4$ [43] with minor amounts of $Cr_2O_3$ [41,50] (**Figure 14b**), while $Cr_2O_3$ was the main constituent of the tribolayer of the conventional compositions ($Cr_3C_2$-25NiCr in **Figure 14a**). These distinct oxide films probably possess different sliding properties, which is displayed by the $Cr_3C_2$-50NiCrMoNb coatings producing slightly higher friction than do the $Cr_3C_2$-25NiCr ones (from 0.35 to 0.40, **Table 5**). The Raman spectra of the tribofilms formed on the $Cr_3C_2$-25NiCr coatings also include a peak at 790 $cm^{-1}$ that could not be undoubtedly identified.

It is also interesting to note that the Raman spectra of the tribofilms differ somewhat from those of the corresponding oxides scale that are spontaneously developed on the coating at 700 °C, outside the wear scar (**Figure 14**). This confirms the occurrence of tribochemical reactions within the tribofilm, i.e. reactions that are not only due to the operating temperature, but also to the additional flash heating occurring at the contact point and to the simultaneous mechanical action by the counterbody. The oxide scale spectra often present broad peaks at around 1360 $cm^{-1}$ and 1580 $cm^{-1}$, which are suspected of belonging to carbon: oxidation of Cr

in the carbide particles probably left an excess C (similar to the observations made for room-temperature wear debris).

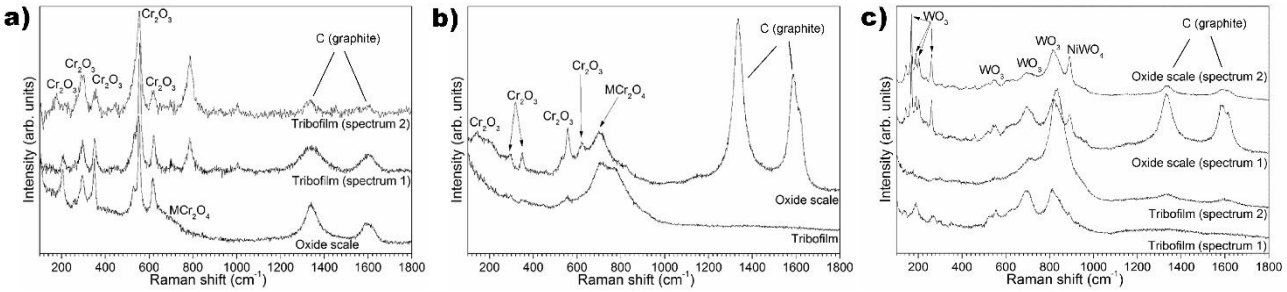


***Figure 14:*** *Raman spectra of the oxide scales outside the wear track and tribofilms of a) $Cr_3C_2$-25NiCr, b) $Cr_3C_2$-50NiCrMoNb and c) $Cr_3C_2$-37WC-18NiCoCr coatings.*

The $Cr_3C_2$-37WC-18NiCoCr coatings exhibited significant degradation of their wear resistance at 700 °C. The main factor causing the high wear rate was the poor oxidation resistance of the WC particles. At lower temperatures, the fine WC particles strengthen the coating structure and provide higher hardness than any of the other tested coatings (**Table 5**). The wear track of the HVAF coating after the high temperature test in **Figure 15a** shows protruding oxidised WC particles, while other areas are covered by a smooth oxide layer hiding most of the structural details of the wear track surface. It is likely that the higher wear rate of the $Cr_3C_2$-37WC-18NiCoCr coatings is caused by the fine WC particles as they i) prevent the formation of uniform tribolayer by protruding from the surface (which also causes slightly higher steady-state friction in comparison to $Cr_3C_2$-25NiCr coatings, **Figure 9** and **Table 5**) and ii) oxidise and lose their strengthening capability. The protruding oxidised WC particles demonstrate that the chromium carbides and chromium-containing matrix did not protect the WC particles from oxidation, neither did the smearing of the wear debris. This becomes evident also from the cross section view in **Figure 15c**, which shows the 1 µm thick oxide layer (pointed out by arrows over the coating surface) on the wear track covering some of the WC particles that have already started oxidising underneath (pointed out by arrows inside the coating). The tribolayer on the wear track was proven to consist of $WO_3$ as a result of the direct oxidation of the WC particles and $NiWO_4$ as a result of reaction with the nickel from the metallic matrix (**Figure 14c**). Even though the extensive oxidation of the WC particles is evident, the high temperature performance and oxidation resistance of this coating is remarkably better than that of the HVOF sprayed WC-CoCr tested at a similar temperature of 750 °C in another study [7] (due to the catastrophic oxidation of the latter). However, the performance is somewhat poorer than that of the previously mentioned HVOF sprayed WC-$(W,Cr)_2C$-Ni coatings. Compared to WC-CoCr, indeed, the currently tested coatings possess significantly lower WC content and even distribution of the WC particles within the coating microstructure, as was previously shown in Section 3.1. However, WC-$(W,Cr)_2C$-Ni was reportedly able [7] to develop a uniform tungstate-based oxide scale (containing no $WO_3$) that covered even the WC particles themselves, preventing their oxidation and allowing the formation of a uniform tribofilm without protrusions. This seems not to occur with the present $Cr_3C_2$-37WC-18NiCoCr, maybe because it does not contain any $(W,Cr)_2C$ mixed carbide phase. The SEM micrograph in **Figure 15b** taken from outside the wear track demonstrates the extensive oxidation of the WC particles compared to the $Cr_3C_2$ particles and the Cr alloyed matrix. The WC particles grow thick oxide clusters while rest of the coating structure forms a layer of fine oxides. The WC particles evidently lose most of their capability to provide improved wear resistance, but on the other hand, they do not cause catastrophic failure of the coating via oxidation, as was the case with the WC-10Co4Cr coating in [7].

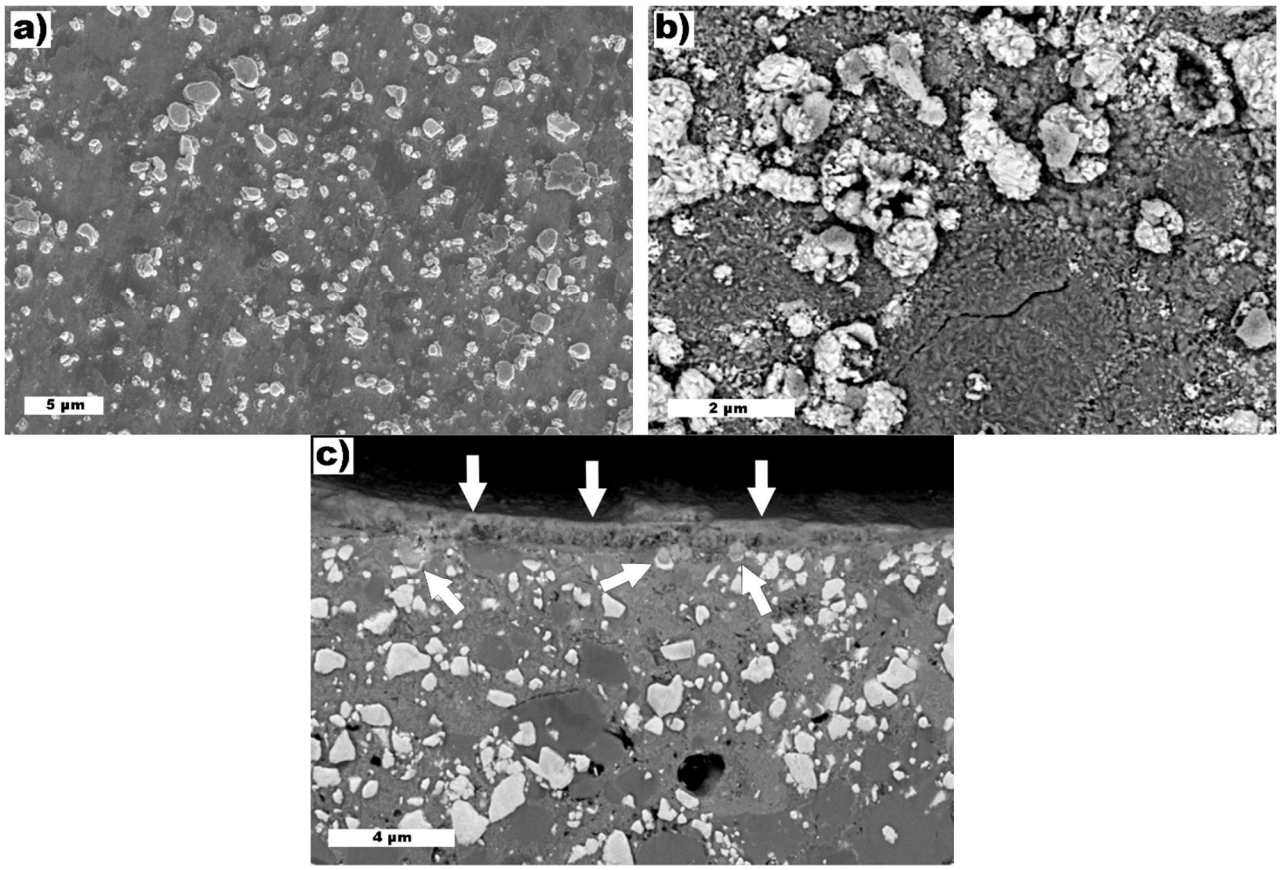


***Figure 15**: SEM images of the HVAF sprayed $Cr_3C_2$-37WC-18NiCoCr coating surface after high temperature ball-on disk test with top-view, a) from the wear track and b) from outside the wear track, and side-view c) from the cross section sample.*

### 3.4. Effect of the Spray Process

The results in Sections 3.2. and 3.3. presented the observed differences in performance between the three coating material compositions: $Cr_3C_2$-25NiCr, $Cr_3C_2$-50NiCrMoNb and $Cr_3C_2$-37WC-18NiCoCr. However, the HVOF and HVAF spray processes differ significantly from each other and produce different particle in-flight properties, i.e. velocity, temperature and melting degree. It is therefore important to compare the coating performance in relation to the spray process.

#### 3.4.1. Room Temperature Behaviour

At room temperature, the spray process seemed to have only a small effect on the coating performance when carrying out the sliding wear tests. Significant differences between the two processes were observed on the coatings produced from the plasma densified $Cr_3C_2$-25NiCr (d) and the $Cr_3C_2$-37WC-18NiCoCr powders. The coefficient of friction values of the former coatings were 0.78 for the HVOF sprayed coating and 0.6 for the HVAF sprayed coating. High value on the HVOF sprayed coating could be caused by the potentially larger wear debris formed during the brittle cracking of the coating surface. While similar cracking was also observed on the HVAF sprayed coating, the coating was sprayed from finer particle size and potentially finer wear debris was formed as the result of the brittle fracture.

In the case of the $Cr_3C_2$-37WC-18NiCoCr material, the HVAF spray process produced a coating with significantly lower wear rates compared to the HVOF sprayed coating. Cracks were observed on the wear track of the HVOF sprayed coating, which indicates a higher probability of material removal by brittle fracture. The HVAF sprayed coating, on the other hand, did not show such behaviour. The main reason for the observed behaviour lies in the process temperature, which in the case of HVOF spraying results in localised brittle areas by overheated particles.

### 3.4.2. High Temperature Behaviour

At 700 °C, the effect of the spray process became more significant compared to the results obtained from the room temperature tests. The wear rates of the HVAF sprayed coatings, besides the $Cr_3C_2$-25NiCr (d) coating, were lower compared to the HVOF sprayed coatings. Especially pronounced difference was observed in the case of the conventional $Cr_3C_2$-25NiCr as significant improvement in wear resistance was measured. One reason for this could be the subsurface cracking of HVOF sprayed $Cr_3C_2$-25NiCr and $Cr_3C_2$-50NiCrMoNb coatings during the test. This cracking of the top layer of the HVOF $Cr_3C_2$-25NiCr coating is evident in **Figure 16b**. The cracks observed in the structure are probably formed by fatigue fracture caused by the continuous loading cycles during the wear test. Such subsurface cracking probably promotes the removal of the tribolayer and subjects the underlying coating material to oxidation and wear. Since the HVAF sprayed coatings proved to maintain the dense structure without similar cracking behaviour, it seems that the uniformity and cohesion of the underlying coating surface plays an important role in the observed behaviour. This enabled the formation of the thick oxide-based tribolayer on the wear track of the HVAF sprayed $Cr_3C_2$-25NiCr coating, seen in **Figure 16a**.

On the other hand, even the HVAF sprayed $Cr_3C_2$-25NiCr (d) coating (**Figure 16c**) experienced sub-surface cracking during sliding wear tests at 700 °C, which is consistent with the higher incidence of tribofilm delamination phenomena (see Section 3.3.2.). This may be due to the fact that the plasma densification process altered deeply the microstructure of the feedstock powder (as was described in Section 3.1) by forming elliptical, elongated $Cr_3C_2$ particles that leave a small matrix mean free path between them. Such microstructural difference is clearly reflected in the resulting coatings (compare **Figure 16c** to **Figures 16a-b**). The low matrix mean free path between the elongated carbide particles clearly impairs the ductility of the coating and facilitates the nucleation and propagation of cracks, particularly when the narrow remaining matrix areas experience significant re-precipitation of secondary carbides at high temperature, as illustrated by the detail of **Figure 16d**. In addition, the metastable $Cr_3C_{2-x}$ ($0 \leq x \leq 0.5$) phase detected in the feedstock powders and as-sprayed coatings was found to transform into a stable carbide form, presumably $Cr_3C_2$, during a 14 h heat treatment experiment done for the powders at 700 °C (XRD patterns in **Figure 17**). The transformation from $Cr_3C_{2-x}$ to $Cr_3C_2$ can decrease the specific volume per Cr atom in the carbide by roughly 2% [39], which might create additional localized tensile stresses or reduce existing compressive stresses. It can also be noticed that in the as-received state the Ni-alloy peaks (at 44.1° and 51.3° in **Figure 17**) of the powders have shifted to lower diffraction angles, which is caused by the substantial increase of Cr content in the alloy [38]. This originates from the melted carbide particles and resulting dissolution of Cr and C into the Ni-alloy during the plasma densification process.

Extensive carbide precipitation can be observed in the microstructure of both HVOF and HVAF sprayed $Cr_3C_2$-25NiCr coatings in **Figure 16**, which indicates substantial carbon content of the metallic matrix in the as-sprayed state. During the high temperature testing, dissolved carbon starts to form fine carbide precipitates with chromium [30]. This behaviour demonstrates that melting of the metal matrix has taken place during the spraying with both processes. Accordingly, significant increase in microhardness was observed for all HVOF sprayed coatings after the high temperature tests. This is related to the carbide precipitations, which can increase the hardness as a result of the short-term heat treatment [38]. This increase was most significant in the case of the HVOF sprayed $Cr_3C_2$-25NiCr (d) and $Cr_3C_2$-37WC-18NiCoCr coatings. The same coatings experienced some brittle cracking during the high temperature testing. Increased microhardness was observed also on the HVAF sprayed coatings from the same materials, while the HVAF sprayed coatings from agglomerated and sintered $Cr_3C_2$-25NiCr and $Cr_3C_2$-50NiCrMoNb powders experienced quite significant drop in microhardness. Apparently, in the latter cases the formation of precipitates resulted in more ductile coating structure, which may result from the fact that, in these coatings, the loss in solid solution strengthening of the C- and Cr-saturated matrix prevails over the effect of secondary carbides precipitation. The heat treatment of similar coatings has accordingly been found to increase the matrix ductility [51]. The reason why the microhardness of the HVAF sprayed $Cr_3C_2$-25NiCr (d) coating was not decreasing during the wear test may actually lie in the state of the feedstock powder. The coating structure is composed of particles with higher melting degree than was actually produced by the HVAF spray process. Instead, the seemingly high melting degree of the particles originates from the plasma densification process, which has already once melted and solidified the majority of the powder particles leaving them partially in a metastable state with high

concentrations of Cr and C in the matrix alloy. Similar reasons related to structure stability could be causing the increase of hardness in the case of both $Cr_3C_2$-37WC-18NiCoCr coatings.

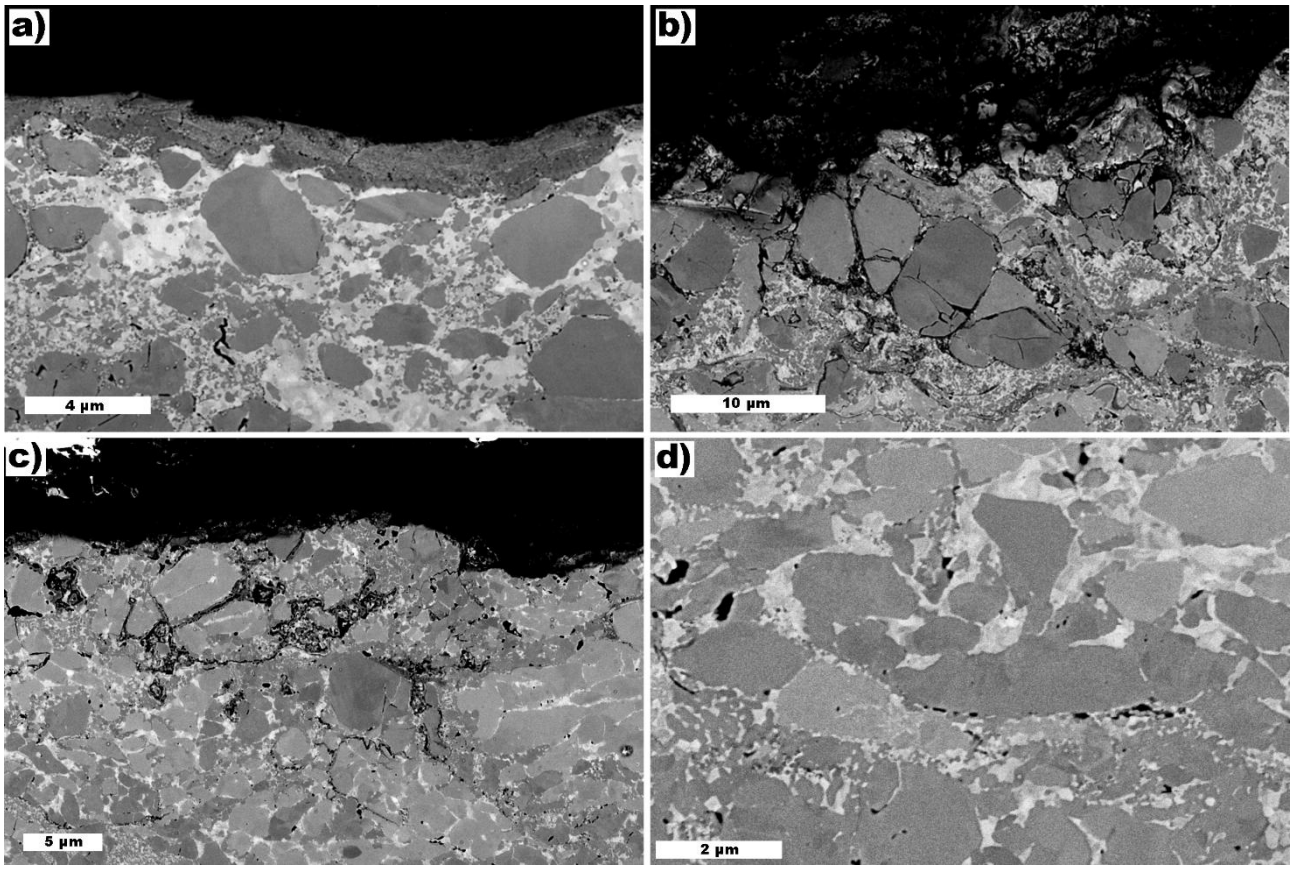


***Figure 16**: SEM micrograph of the wear track cross section of a) HVAF and b) HVOF sprayed $Cr_3C_2$-25NiCr coatings, and of c) HVAF sprayed $Cr_3C_2$-25NiCr coating from plasma densified powder, with d) detail of secondary carbides precipitation within the NiCr matrix.*

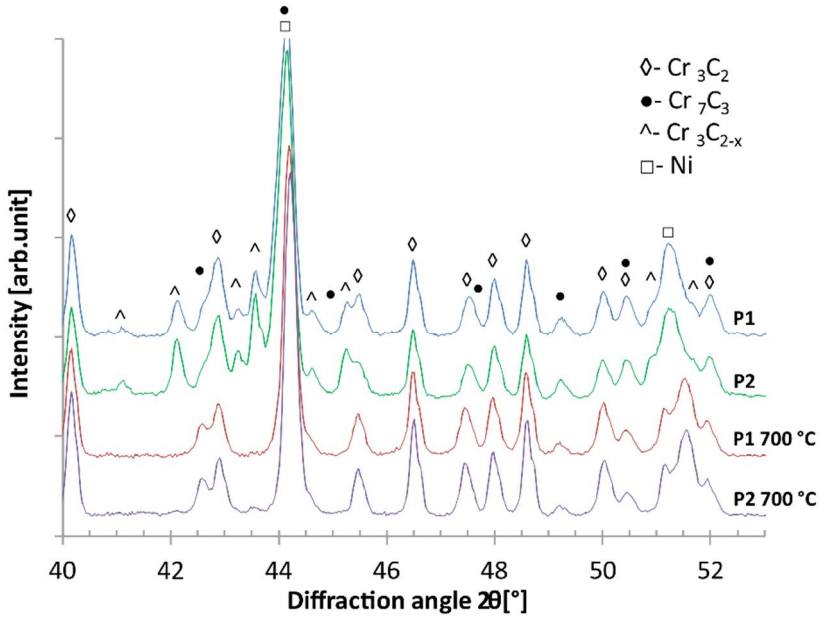


***Figure 17**: Measured XRD patterns from the as-received plasma densified powders for HVOF (P1) and HVAF (P2) processes, and from powders after heat treatment at 700 °C (P1 700 °C and P2 700 °C).*

## 4. CONCLUSIONS

Various $Cr_3C_2$-based coatings were produced with HVOF and HVAF thermal spray processes: $Cr_3C_2$-25NiCr, $Cr_3C_2$-50NiCrMoNb and $Cr_3C_2$-37WC-18NiCoCr. The sliding wear behaviour was tested at room temperature and at 700 °C by a tribometer with a ball-on-disk configuration. Alumina ball was used as the counterpart. The following conclusions were made from the presented results:

- At room temperature, the coatings produced very similar values of the coefficient of friction. The highest (0.78) and lowest (0.60) values were observed on HVOF and HVAF sprayed $Cr_3C_2$-25NiCr (d) coatings, respectively. The same coatings experienced also the highest wear rates due to brittle cracking of the coating material. The lowest wear rate was achieved with the $Cr_3C_2$-37WC-18NiCoCr coatings due to the hard WC particles.
- The wear mechanism was similar for all coatings, a combination of i) abrasive grooving, ii) brittle fracture, iii) delamination and iv) tribo-oxidation. Poorly crystalline oxide clusters and small debris particles were observed on all surfaces. The amorphous nature of the oxidised debris clusters is considered to be one of the causes of the relatively high ($\geq 0.6$) friction coefficient produced by these coatings in the present test conditions.
- At 700 °C, significantly lower coefficients of friction (0.35-0.48) were achieved for all the tested coatings, compared to the room temperature tests. The decreased coefficient of friction values were the result of crystalline, oxide based tribolayers on the wear tracks. The tribolayers of $Cr_3C_2$-25NiCr coatings consisted of $Cr_2O_3$ while the tribolayer on $Cr_3C_2$-50NiCrMoNb coatings mainly contained $NiCr_2O_4$. The coatings containing WC formed a discontinuous tribolayer, whose uniformity is impaired by the growth of $WO_3$ protrusions over WC particles.
- The $Cr_3C_2$-25NiCr coatings experienced similar or even lower wear rates at high temperature than at room temperature. The lowest wear rate was measured for the HVAF sprayed $Cr_3C_2$-25NiCr coating. The $Cr_3C_2$-50NiCrMoNb coatings, on the other hand, experienced higher wear rate due to higher matrix content and the $Cr_3C_2$-37WC-18NiCoCr coatings suffered from the rapid oxidation of WC particles preventing the formation of a uniform tribolayer.
- Subsurface cracking took place in HVOF sprayed coatings of $Cr_3C_2$-25NiCr and $Cr_3C_2$-50NiCrMoNb during the high temperature sliding tests. The HVAF sprayed counterparts did not show the same behaviour, which was beneficial for maintaining the tribolayer intact and for decreasing the wear rate. On the other hand, the $Cr_3C_2$-25NiCr coatings obtained from the plasma densified feedstock exhibited sub-surface cracking regardless of the deposition technique. This is due to the sprayed coating retaining the powder microstructure induced by the plasma densification process, which features particularly low matrix mean free path between elongated carbide grains. In addition to that, secondary carbides precipitation within the matrix at high temperature also contributes to increased brittleness at high temperature.
- All tested coatings performed well under sliding wear conditions and have great potential as wear resistant coatings at room temperature and elevated temperature.

## 5. ACKNOWLEDGEMENTS

This research was carried out as part of the DIMECC's (Digital, Internet, Materials & Engineering Co-Creation) Hybrid Materials program. We gratefully acknowledge the financial support from Tekes and the participating companies. The authors would also like to thank Mr. Mikko Kylmälahti of Tampere University of Technology for his help with the spray processing of the coatings.

## 6. REFERENCES


[1] W. Tillman, E. Vogli, Selecting surface-treatment technologies, in: F.-W. Bach, K. Möhwald, A. Laarmann, T. Wenz (Eds.), Mod. Surf. Technol., Wiley-VCH, 2006: pp. 1–10.

[2] P. Vuoristo, Thermal Spray Coating Processes, in: Comprehensive Materials Processing, Elsevier, 2014.

[3] L.M. Berger, Application of hardmetals as thermal spray coatings, Int. J. Refract. Met. Hard Mater. 49 (2015) 350–364.

[4] Š. Houdková, F. Zahálka, M. Kašparová, L.M. Berger, Comparative study of thermally sprayed coatings under different types of wear conditions for hard chromium replacement, Tribol. Lett. 43 (2011) 139–154.

[5] A. Wank, B. Wielage, H. Pokhmurska, E. Friesen, G. Reisel, Comparison of hardmetal and hard chromium coatings under different tribological conditions, Surf. Coat. Technol. 201 (2006) 1975–1980.

[6] V.B. Voitovich, V. V. Sverdel, R.F. Voitovich, E.I. Golovko, Oxidation of WC-Co, WC-Ni and WC-Co-Ni Hard Metals in the Temperature Range 500-800 °C, Int. J. Refract. Met. Hard Mater. 14 (1996) 289–295.

[7] G. Bolelli, L.M.L.-M. Berger, M. Bonetti, L. Lusvarghi, Comparative study of the dry sliding wear behaviour of HVOF-sprayed WC-$(W,Cr)_2C$-Ni and WC-CoCr hardmetal coatings, Wear. 309 (2014) 96–111.

[8] G. Bolelli, L.-M. Berger, T. Börner, H. Koivuluoto, V. Matikainen, L. Lusvarghi, et al., Sliding and abrasive wear behaviour of HVOF- and HVAF-sprayed $Cr_3C_2$-NiCr hardmetal coatings, Wear. 358–359 (2016) 32–50.

[9] R.F. Voitovich, E.A. Pugach, High-temperature oxidation characteristics of the carbides of the Group VI transition metals, Sov. Powder Metall. Met. Ceram. 12 (1973) 314–318.

[10] L. Pawlowski, The Science and Engineering of Thermal Spray Coatings, 2nd ed., John Wiley & Sons, 2008.

[11] S. Zimmermann, B. Gries, B. Brüning, New Cermet Powders for HVOF Spraying with Improved Corrosion and Oxidation Resistance for offshore, mining and power generation applications, Therm. Spray Bull. 2 (2011) 94–100.

[12] I. Hulka, V.A. Şerban, I. Secoşan, P. Vuoristo, K. Niemi, Wear properties of CrC-37WC-18M coatings deposited by HVOF and HVAF spraying processes, Surf. Coat. Technol. 210 (2012) 15–20.

[13] A. Määttä, U. Kanerva, P. Vuoristo, Structure and tribological characteristics of HVOF coatings sprayed from powder blends of $Cr_3C_2$-25NiCr and NiCrBSi alloy, J. Therm. Spray Technol. 20 (2011) 366–371.

[14] J.M. Guilemany, N. Espallargas, J. Fernández, P.H. Suegama, A.V. Benedetti, High-velocity oxyfuel $Cr_3C_2$-NiCr replacing hard chromium coatings, J. Therm. Spray Technol. 14 (2005) 335–341.

[15] M. Roy, A. Pauschitz, R. Polak, F. Franek, Comparative evaluation of ambient temperature friction behaviour of thermal sprayed $Cr_3C_2$–25(Ni20Cr) coatings with conventional and nano-crystalline grains, Tribol. Int. 39 (2006) 29–38.

[16] L.M. Berger, M. Woydt, S. Saaro, Comparison of self-mated hardmetal coatings under dry sliding conditions up to 600 °C, Wear. 266 (2009) 406–416.

[17] D. Poirier, J.G.J.-G. Legoux, R.S.S. Lima, Engineering HVOF-Sprayed $Cr_3C_2$-NiCr Coatings: The Effect of Particle Morphology and Spraying Parameters on the Microstructure, Properties, and High Temperature Wear Performance, J. Therm. Spray Technol. 22 (2013) 280–289.

[18] G. Bolelli, B. Bonferroni, J. Laurila, L. Lusvarghi, A. Milanti, K. Niemi, et al., Micromechanical properties and sliding wear behaviour of HVOF-sprayed Fe-based alloy coatings, Wear. 276–277 (2012) 29–47.

[19] A.S.M. Ang, H. Howse, S.A. Wade, C.C. Berndt, Development of Processing Windows for HVOF Carbide-Based Coatings, J. Therm. Spray Technol. 25 (2016) 28–35.

[20] T. Varis, T. Suhonen, A. Ghabchi, A. Valarezo, S. Sampath, X. Liu, et al., Formation mechanisms, structure, and properties of HVOF-sprayed WC-CoCr coatings: An approach toward process maps, J. Therm. Spray Technol. 23 (2014) 1009–1018.

[21] G. Bolelli, L.-M. Berger, T. Börner, H. Koivuluoto, L. Lusvarghi, C. Lyphout, et al., Tribology of HVOF- and HVAF-sprayed WC-10Co4Cr hardmetal coatings: A comparative assessment, Surf. Coat. Technol. 265 (2015) 125–144.

[22] A. Verstak, V. Baranovski, Activated Combustion HVAF Coatings for Protection against Wear and

High Temperature Corrosion, in: C. Moreau, B.R. Marple (Eds.), Therm. Spray 2003 Adv. Sci. Appl. Technol., ASM International, Materals Park, OH, USA, 2003: pp. 535–541.
[23] S.G. Davis, C.K. Law, Determination of and Fuel Structure Effects on Laminar Flame Speeds of C1 to C8 Hydrocarbons, Combust. Sci. Technol. 140 (1998) 427–449.
[24] H. Kreye, S. Zimmermann, P. Heinrich, The role of the fuel gas in the HVOF process, in: Proc. ITSC'95, 1995: pp. 393–398.
[25] H. Katanoda, K. Sakata, K. Tagomori, N. Sugiyama, S. Sasaki, Y. Shinya, et al., PIV Measurement and Numerical Simulation of the Particle Velocity in a HVAF Spray, in: Int. Therm. Spray Conf., 2014: pp. 946–949.
[26] V. Matikainen, K. Khanlari, A. Milanti, H. Koivuluoto, P. Vuoristo, Spray parameter effect on HVAF sprayed (Fe,Cr)C-30FeNiCrSi hardmetal coatings, in: Int. Therm. Spray Conf. 2016, 2016: pp. 184–189.
[27] V. Matikainen, H. Koivuluoto, P. Vuoristo, Microstructural characteristics of different $Cr_3C_2$ coating compositions sprayed with HVOF and HVAF processes, in: 28th Int. Conf. Surf. Modif. Technol., Valardocs, 2015: pp. 77–87.
[28] S. Matthews, B. James, M. Hyland, High temperature erosion of $Cr_3C_2$-NiCr thermal spray coatings - The role of phase microstructure, Surf. Coat. Technol. 203 (2009) 1144–1153.
[29] S. Matthews, B. James, M. Hyland, The role of microstructure in the mechanism of high velocity erosion of $Cr_3C_2$-NiCr thermal spray coatings: Part 1 - As-sprayed coatings, Surf. Coat. Technol. 203 (2009) 1086–1093.
[30] S. Matthews, M. Hyland, B. James, Long-Term Carbide Development in High-Velocity Oxygen Fuel/High-Velocity Air Fuel $Cr_3C_2$-NiCr Coatings Heat Treated at 900°C, J. Therm. Spray Technol. 13 (2004) 526–536.
[31] Q. Wang, S. Zhang, Y. Cheng, J. Xiang, X. Zhao, G. Yang, Wear and corrosion performance of WC-10Co4Cr coatings deposited by different HVOF and HVAF spraying processes, Surf. Coat. Technol. 218 (2013) 127–136.
[32] C. Lyphout, S. Björklund, M. Karlsson, M. Runte, G. Reisel, P. Boccaccio, Screening Design of Supersonic Air Fuel Processing for Hard Metal Coatings, J. Therm. Spray Technol. 220 (2014).
[33] G. Bolelli, T. Börner, A. Milanti, L. Lusvarghi, J. Laurila, H. Koivuluoto, et al., Tribological behavior of HVOF- and HVAF-sprayed composite coatings based on Fe-Alloy+WC–12% Co, Surf. Coat. Technol. 248 (2014) 104–112.
[34] L.-M. Berger, R. Trache, F.-L. Toma, S. Thiele, J. Norpoth, L. Janka, Development of cost-effective hardmetal coating solutions for high-temperature applications, Part one: Feedstock powders, cost-effectiveness and coating properties, Therm. Spray Bull. 8 (2015) 126–136.
[35] V. Matikainen, K. Khanlari, A. Milanti, H. Koivuluoto, P. Vuoristo, Spray parameter effect on HVAF sprayed (Fe,Cr)C-30FeNiCrSi hardmetal coatings, in: Int. Therm. Spray Conf. 2016, 2016: pp. 184–189.
[36] C.A. Schneider, W.S. Rasband, K.W. Eliceiri, NIH Image to ImageJ: 25 years of image analysis, Nat. Methods. 9 (2012) 671–675.
[37] J. Kreisel, M.C. Weber, N. Dix, F. Sánchez, P.A. Thomas, J. Fontcuberta, Probing individual layers in functional oxide multilayers by wavelength-dependent raman scattering, Adv. Funct. Mater. 22 (2012) 5044–5049.
[38] S. Matthews, L.-M. Berger, Long-term compositional/microstructural development of $Cr_3C_2$-NiCr coatings at 500°C, 700°C and 900°C, Int. J. Refract. Met. Hard Mater. 59 (2016) 1–18.
[39] E. Bouzy, E. Bauer-Grosse, G. Le Caer, NaCl and filled $Re_3B$-type structures for two metastable chromium carbides.pdf, Philos. Mag. B. 68 (1993) 619–638.
[40] C.J. Li, G.C. Ji, Y.Y. Wang, K. Sonoya, Dominant effect of carbide rebounding on the carbon loss during high velocity oxy-fuel spraying of $Cr_3C_2$-NiCr, Thin Solid Films. 419 (2002) 137–143.
[41] L.J. Oblonsky, T.M. Devine, A surface enhanced Raman spectroscopic study of the passive films formed in borate buffer on iron, nickel, chromium and stainless steel, Corros. Sci. 37 (1995) 17–41.
[42] F. Tuinstra, L. Koenig, Raman Spectrum of Graphite, J. Chem. Phys. 53 (1970) 1126–1130.
[43] M. da Cunha Belo, M. Walls, N.E.E. Hakiki, J. Corset, E. Picquenard, G. Sagon, et al., Composition, structure and properties of the oxide films formed on the stainless steel 316L in a primary type PWR environment, Corros. Sci. 40 (1998) 447–463.
[44] M.F. Daniel, B. Desbat, J.C. Lassegues, B. Gerand, M. Figlarz, Infrared and Raman study of WO3 tungsten trioxides and WO3·xH2O tungsten trioxide hydrates, J. Solid State Chem. 67 (1987) 235–247.

[45] M. Gotić, M. Ivanda, S. Popović, S. Musić, Synthesis of tungsten trioxide hydrates and their structural properties, Mater. Sci. Eng. B Solid-State Mater. Adv. Technol. 77 (2000) 193–201.
[46] A. Kuzmin, R. Kalendarev, A. Kursitis, J. Purans, Confocal spectromicroscopy of amorphous and nanocrystalline tungsten oxide films, J. Non. Cryst. Solids. 353 (2007) 1840–1843.
[47] P. Porta, G. Minelli, I. Pettiti, L.I. Botto, H.J. Thomas, Anderson phases as precursors of nickel-molybdenum-tungsten oxides, J. Mater. Chem. 7 (1997) 311–313.
[48] J.A.R. Wesmann, S. Kuroda, N. Espallargas, The Role of Oxide Tribofilms on Friction and Wear of Different Thermally Sprayed WC-CoCr, J. Therm. Spray Technol. 26 (2017) 492–502.
[49] G. Bolelli, A. Candeli, L. Lusvarghi, A. Ravaux, K. Cazes, A. Denoirjean, et al., Tribology of NiCrAlY+$Al_2O_3$ composite coatings by plasma spraying with hybrid feeding of dry powder+suspension, Wear. 344–345 (2015) 69–85.
[50] J. Mougin, T. Le Bihan, G. Lucazeau, High-pressure study of $Cr_2O_3$ obtained by high-temperature oxidation by X-ray diffraction and Raman spectroscopy, J. Phys. Chem. Solids. 62 (2001) 553–563.
[51] L. Janka, J. Norpoth, R. Trache, L.-M. Berger, Influence of heat treatment on the abrasive wear resistance of a $Cr_3C_2$-NiCr coating deposited by an ethene-fuelled HVOF spray process, Surf. Coat. Technol. 291 (2016) 444–451.